Transmission Performance Improvements in Radio-to-Optic Direct Conversion Network Systems

Pat Suwonpanich

Graduate School of Engineering
Osaka University

December, 2000

To my loving parents,
and sisters

Acknowledgements

This research has been carried out during my Ph.D. course pursued at Department of Communications Engineering, Graduate School of Engineering, Osaka University.

I would like to express my deepest appreciation to Prof. Shozo Komaki for his supervision, continuing encouragement, valuable discussions, academic advice, and various supports throughout this research.

I am much indebted to Prof. Ken-ichi Kitayama of the Department of Electronics and Information Systems, Graduate School of Engineering, Osaka University, for his reading and valuable criticism on the whole contents of this thesis.

I am deeply grateful to Prof. Norihiko Morinaga, Prof. Hajime Maeda, Prof. Toshiyuki Shiozawa, Prof. Hiromasa Ikeda of the Department of Communications Engineering, and Prof. Hiroshi Motoda of Intelligent Systems Science Division, for their creative comments for this research.

I am also indebted to Associate Prof. Seiichi Sampei, Associate Prof. Masayuki Matsumoto, Associate Prof. Yoji Iiguni, and Associate Prof. Miki Yamamoto of the Department of Communications Engineering, Associate Prof. Shinsuke Hara of the Department of Electronics and Information Systems, Associate Prof. Takashi Washio of the Institute of Scientific and Industrial Research, and all academic lecturers at the Department of Communications Engineering, Graduate School of Engineering for their valuable comments for this research.

I would like to express my sincere appreciation to Associate Prof. Minoru Okada of Nara Institute of Science and Technology, Mr. Yukinori Suda of NEC corporation C&C Media Research Labs., Dr. Yozo Shoji of Yokosuka radio communications research center, communications research laboratory (CRL), and Dr. Masahiro Nishi of Hiroshima City University for their valuable discussions and comments throughout this research.

I also appreciate all members of Komaki Laboratory for their useful advice for this research, especially Mr. Kazuo Kumamoto and Mr. Ryo Inohara for their helpful discussions.

I am deeply indebted to Prof. Prasit Prapinmongkolkarn of Chulalongkorn University, Thailand, who kindly recommended and introduced me to Komaki laboratory.

I am heartily thankful to my family, including my father, mother, and sisters for their understanding to me, enabling me to conduct the research without worry.

I wish to thank my Thai and Japanese friends, especially Miss Wararat Boonchuduang for her encouragement during my hard time.

I also would like to acknowledge Asia Japan Alumni (ASJA) International for granting me the scholarship to pursue the Ph.D. course.

Last, but by no means least, I would like to express my deep sense of appreciation to Associate Prof. Katsutoshi Tsukamoto for his helpful discussions, various academic comment, untiring efforts in guidance, and continuing encouragement from the beginning to the end of this research.

Pat Suwonpanich

December, 2000

Preface

This thesis presents transmission performance improvements in radio-on-fiber network systems using radio-to-optic direct conversion schemes. It is an outcome of the research done during the Ph.D. course pursued at Department of Communications Engineering, Graduate School of Engineering, Osaka University.

The thesis is organized in five chapters as follows.

Chapter 1 addresses the background of the research on the radio-on-fiber network system and its optical modulation schemes including the radio-to-optic direct conversion (ROC) scheme. The necessity of a research on techniques to reduce intermodulation distortions in the systems is explained. Also, the objective and scope of the thesis are briefed.

Chapter 2 describes the radio-on-fiber network system using the ROC scheme, which is termed "radio-to-optic direct conversion network system" here, in detail. The concept and characteristics of the network, its multiplexing schemes, and the ROC scheme are addressed. Also, nonlinear modulation characteristics of the ROC scheme is discussed and the problem caused by the nonlinear modulation characteristics in the systems transporting radio frequency (RF) subcarrier multiplexing (SCM) signals is clarified.

Chapter 3 proposes the ROC network systems for the case of transmitting the RF SCM signals. The ROC/heterodyne detection (HD) system and ROC/self-heterodyne detection (SHD) system are introduced and the carrier-to-distortion-plus-noise power ratio (CDNR) performance is theoretically analyzed taking into account the intermodulation distortion. The CDNR performance and spurious-free dynamic range (SFDR) performance of the ROC/HD and ROC/SHD systems are discussed. Also, performance improvements by both of the ROC systems are evaluated by comparing with the conventional intensity modulation and single-sideband modulation systems.

Chapter 4 presents novel cascaded ROC network systems which resolve a problem of intermodulation distortion occurring in the conventional cascaded systems and a problem of beat noise occurring in the systems employing star-type or bus-type inter-cell connection link. The concept of the proposed cascaded systems is explained and the carrier-to-noise ratio (CNR) performances of the cascaded ROC/HD system and cascaded ROC/SHD system are theoretically analyzed and discussed. Also, the optimization of the optical modulation

index in each radio base station is proposed. Performance improvements by the proposed cascaded ROC systems are evaluated by comparing with the conventional cascaded intensity modulation system.

Chapter 5 draws the conclusions of this thesis by summarizing the results of transmission performance improvements achieved by the proposed radio-to-optic direct conversion network systems.

Contents

List of Figures

Chapter 1

Introduction

In a cellular mobile communication system, the coverage area is divided into cells, where the radio base stations (RBSs) housing the transmitting/receiving antennas and associated equipment are located. Each control station (CS) controls a number of RBSs through an interconnecting network of high-speed data and voice links between RBSs and the CS. In order to meet the rapidly increasing demand for mobile communications, microcellular systems have been extensively studied and employed. The systems contain smaller cells (microcells) and promise effective frequency utilization, thus serve more subscribers and satisfy the escalating demand. However, as a microcell size shrinks in order to accommodate more and more subscribers, a larger number of RBSs are required to cover a given area. Furthermore, the number of RBSs has been increased in order to start new kinds of radio service including a combination of services such as voice, data, fax, and video. System providers must use a RBS density of tens, hundreds, or even thousands of RBSs per square kilometers to provide such enhanced services with high quality of service.

Therefore, it is essential to develop simpler RBSs. Radio-on-fiber systems have been extensively researched recently to transmit radio frequency (RF) signals via fiber-optic networks [1]-[7]. In radio-on-fiber systems, a large number of RBSs are connected via optical fiber to the CS located at an economical location. RF signals in micro-cells are encapsulated into an optical signal envelope and then transmitted to their destinations through fibers.

The advantages of the radio-on-fiber system are noted below:

1) Concerning RBS

(1.1) Cost saving: All of baseband modulators/demodulators and system control circuitry are relocated away from the RBS to the CS, so the RBS can be much smaller and consumes less power. This results in a great saving in real estate and building costs. Furthermore, since the baseband modulation and demodulation are not implemented

in the RBSs, therefore the RBSs and backyard fiber-optic networks can be used for various types of radio services flexibly, so the number of RBSs can be much reduced.

(1.2) Reliability and Maintainability: With less circuitry, the reliability and maintainability is increased.

2) Service enhancement: all the system control functions and diversity combining/switching functions can be performed in one centralized location, i.e. a CS, resulting in an enhancement in service quality.

3) Modulation-independent: Since the link is transparent to RF signals, it is independent of the modulation format used. It can be used for either analog signals or digital signals.

4) Scalability: New cells can be easily added to the network to provide increased capacity through cell splitting to meet increased demand.

5) Service Upgrade and Maintenance: Repairs and service upgrades at a centralized location are most convenient and cost effective.

6) Dynamic RF carrier allocation and synchronization: Dynamic RF carrier allocation and synchronization can potentially be implemented from a centralized location.

Radio-on-fiber systems have been demonstrated using UHF-band subcarrier frequencies which are transmitted via optical fiber and then subsequently propagated within a microcell zone. Commercially available optical devices have been successfully utilized to demonstrate these low frequency fiber optic microcellular mobile systems [7],[8].

The primary disadvantage of this infrastructure is that the signal transverses the fiber in analog form. Since detection of the desired voice/data is not performed until the RF signal is received at the CS or RBS, the noise and nonlinearities generated by the optical transmitter, fiber, and receiver will combine with interference and multipath from the wireless environment to degrade system quality of service. The severity of this performance degradation determines the performance requirements which must be met by the optical devices used in the infrastructure.

Regarding optical modulation/detection schemes for radio-on-fiber systems, an analog intensity modulation/direct detection (IM/DD) scheme has been mainly considered from the viewpoint of its technical and economical implementation [9]-[11]. However, in the conventional IM scheme, an optical spectrum consisting of the carrier with sidebands on both sides of the carrier is generated. When these signals are transmitted over an optical fiber, each frequency component experiences a different phase shift due to fiber chromatic

dispersion. Phase differences between the carrier and each of the optical sidebands can cause the beat signals at the photodiode to destructively interfere, nulling the post-detection RF power. For instance, when an RF signal at 28 GHz is transported over standard single-mode fiber at 1550 nm, the link distance is limited to only 3 km, and at 60 GHz the distance is less than 1 km [12].

Moreover, it is foreseen that the demands for high-bit-rate multimedia wireless services based on wireless ATM will grow in the not-too-distant personal communications [13]-[18]. Therefore, more superior transmission quality will be required for the optical link in radio-on-fiber system. In addition, the long-haul radio-on-fiber link needed for globally enhanced wide area networks requires high-quality and low distortion optical transmission. A feasible solution to improve the optical link quality is coherent optical transmission systems in which the signal and the local oscillator are mixed in a receiver to obtain optical-to-electrical conversion. The coherent systems can approach the shot noise limited performance, make up considerably-dense optical frequency division multiplexing signals, and also can detect frequency or phase of the optical carrier. Another distinctive feature of coherent systems is the transparency of signaling formats between radio links and optical links. For instance, if we generate optical QPSK signals, then we can regenerate QPSK signals in the RF band easily by use of optical heterodyne detection. The coherent optically-fed systems have been widely researched to realize the millimeter-wave distribution in broadband wireless local loop systems [19],[20].

Chapter 2 is devoted to review principles, characteristics and advantages of a coherent radio-on-fiber system employing radio-to-optic direct conversion (ROC) scheme [21],[22]. The ROC scheme utilizes a single electro-optic crystal to simulate the action of a rotating birefringent plate which, when acting upon a circularly polarized light beam, can produce a separable component shifted in frequency. In other words, the ROC scheme is one of optical single-sideband (SSB) modulation techniques. The merit of the scheme is that no harmonics are generated. This is due to the fact that its output amplitude is a nonlinear function of the amplitude of the RF signal, not the function of the instantaneous value. Therefore, only nonlinear distortion in the output amplitude arises and no sidebands other than the first-order sideband are generated. RF power nulls at the receiver and the dispersion penalty when transporting high frequency signals over fiber can be remarkably reduced using optical SSB modulation [23],[12]. In this chapter, nonlinear modulation characteristics of the ROC scheme is investigated and compared with those of the conventional optical modulation

schemes.

Multiplexing schemes in radio-on-fiber systems are also discussed in Chapter 2. Subcarrier multiplexing (SCM) scheme is one of promising schemes and has been extensively researched and developed recently in order to transport frequency division multiplexing (FDM) RF signals over optical fiber in radio-on-fiber systems such as the fiber-optic microcellular communication system, the optically-distributed millimeter-wave wireless system and so on [24]-[27]. Such systems support RF signals without the need for any multiplexing equipment. In the SCM system, the optical source or the optical carrier is modulated by RF FDM signals which produce subcarriers of the optical carrier. Each subcarrier can be independently modulated using any conventional modulation format, e.g. FM, AM, FSK, PSK. Thus the optical carrier is capable of supporting multiple channels simultaneously without the need for complicated time, laser wavelength or code division. In the SCM system, however, the nonlinear modulation characteristic of the optical modulation leads to intermodulation distortion by which the system performance deteriorates. The performance of the ROC systems transporting single carrier RF QPSK and QAM signals was analyzed and discussed in Ref. [21].

The first object of this study is to investigate the SCM coherent radio-on-fiber systems employing the ROC scheme taking into account their nonlinear modulation characteristics. Such systems are proposed and examined in Chapter 3 [28],[29]. The SCM ROC system can convert multicarrier RF signals into optical FDM signals with the same modulation format and frequency intervals. SCM SSB systems may also be realized by dual Mach-Zehnder Interferometer (DMZ) type [30] and Cascaded Phase Modulator (CPM) type [31]-[33] optical SSB-suppressed carrier modulators. Since ROC scheme also generates the pilot carrier component, not only heterodyne detection (HD), but also self-heterodyne detection (SHD) can be realized. Degradation in carrier-to-distortion-plus-noise power ratio (CDNR) performance due to the effect of intermodulation distortions in each system is theoretically analyzed. The received CDNR performance [28] and spurious-free dynamic range (SFDR) performance [29] of the ROC/HD and ROC/SHD systems are discussed. Also, the performance improvements by the SCM ROC systems are evaluated by comparing with the conventional SSB modulation systems and the intensity modulation system.

Regarding inter-cell connection link configuration, radio-on-fiber systems employing star-type link [34],[35] and bus-type link [36],[37] have been widely studied. However, beat noises occur in both star-type and bus-type systems because multiple laser diodes (LD) are used.

Consequently, the optical transmission performance is severely deteriorated. Wavelength division multiplexing (WDM) technique can solve this problem, however, this technique requires complicated control of wavelengths of the laser.

Another solution to this problem is to employ a cascade-type inter-cell connection link. The cascaded IM/DD scheme and cascaded phase modulation (PM)/HD scheme have been proposed and studied [38],[39]. However, transmission performance of these conventional cascade-type link systems suffers severely from the intermodulation distortion even if only one RF subcarrier is used per RBS and a linearized optical modulator is employed, since all of the optical carrier and signals from previous RBSs are modulated together in the RBS.

The second object of this study is to investigate and improve the performance of the cascade-type link configuration in which no intermodulation distortion occurs. Chapter 4 proposes novel cascaded radio-on-fiber systems [40]-[44]. In the uplink of the proposed cascaded systems, the optical pilot carrier is divided from all signals modulated by RF signals at previous RBSs by using a frequency splitter. After that, the optical modulator converts a RF signal at the current RBS to an optical signal by modulating only the pilot carrier component. Then, by the use of a frequency combiner, the optical carrier and all optical signals are combined together again. Therefore, no intermodulation distortion due to cascaded modulators occurs in the systems. Also, no beat noise caused by the use of multiple light sources occurs. In order to improve the performance of the proposed ROC system, the optimization of the optical modulation index in each RBS is proposed [40],[43]. The carrier-to-noise ratio (CNR) performance of the cascaded ROC/HD system and cascaded ROC/SHD system are theoretically analyzed and compared with that of conventional cascaded systems.

Chapter 5 summarizes all the conclusions obtained in this thesis.

Chapter 2

Radio-to-Optic Direct Conversion Network

2.1 Introduction

A radio-on-fiber network using radio-to-optic direct conversion (ROC) scheme is termed radio-to-optic direct conversion network here. Radio-on-fiber networks are optical backbone networks for transporting RF signals to remote RBSs without any baseband modulation/demodulation. In general, therefore, analog optical modulation techniques are employed in the radio-on-fiber networks. Such systems have several advantages over the conventional microcellular mobile systems such as cost saving on RBSs, service enhancement, modulation-independent, network flexibility, convenient service upgrade, and suitability for dynamic RF carrier allocation and synchronization.

Consequently, the radio-on-fiber networks are considered as a promising candidate for various radio access networks such as future public wireless communication systems (IMT 2000) [45], wireless local area networks (wireless LAN), roadside-to-vehicle radio access link in intelligent transport systems (ITS) [46], or distribution systems of cable television signals (CATV) [47].

However, there are problems such as the effect of fiber chromatic dispersion in radio-on-fiber systems employing the conventional intensity modulation/direct detection (IM/DD) scheme. The ROC scheme, which is one of optical single-sideband (SSB) modulation technique, can overcome the effect of fiber chromatic dispersion and can be employed in coherent systems where the transmission performance is improved over IM/DD systems. Section 2.2 describes the concept of the ROC network in detail, discusses the multiplexing schemes, and clarifies characteristics and problems in IM/DD systems. Section 2.3 introduces the principle of ROC scheme, discusses its nonlinear modulation characteristics, and addresses the reason why the performance of the ROC systems in the case of transporting subcarrier multiplexing RF signals has to be examined.

2.2 Radio-on-Fiber Network

The concept of the radio-on-fiber network is illustrated in Fig. 2.1. In the uplink, a terminal transmits information signals to the RBS via RF link, then, in an optical link, an optical modulator in each RBS converts the RF signals into optical signals, and the optical signals are transmitted to a control station (CS) via fiber. The advantages of the optical fiber are suitability for high frequency and wideband, low transmission loss, interference-immune signal distribution, and so on. At a receiver in the CS, the optical-to-electrical (O/E) conversion is performed, and, finally, the RF signals are regenerated. In the downlink, the reverse operation is implemented. The RBS, which is an interface receiving or radiating the RF signals in each radio zone, is mainly equipped with only the apparatus that performs electrical-to-optical (E/O) and O/E conversions. The CS performs the functions of radio modulation/demodulation and other controls such as channel allocations.

Therefore, the RBS becomes much simpler. In addition, since there is no baseband modulation/demodulation in the RBS, the RBS is independent of RF signal formats and can provide universal radio access links that are available to any type of RF signals. The concentrated implementation of complex functions in the CS provides simplified and cost-effective constructions of the network. It is also suitable for realization of advanced techniques such as a macro diversity and hand-over control [48].

Regarding multiplexing schemes, the candidates are subcarrier multiplexing (SCM), time division multiplexing (TDM), wavelength division multiplexing (WDM), and code division multiplexing (CDM). The advantage of TDM is no generation of optical beat noise caused by the use of several optical sources. However, the disadvantage of TDM is the requirement of synchronization control among RBSs. Several CDM schemes such as frequency spread code division multiplexing [49] and time spread code division multiplexing [50] have also been investigated because of their easy applicability to random access networks. However, there are the difficulty of high-speed code synchronization between a transmitter and a receiver, and very fast operation of photonic device for coding. The WDM scheme is a promising scheme in high-bit-rate digital transmission systems, and its advantages are effective use of many available wavelengths and no generation of optical beat noise caused by the use of several optical sources. However, it is not suitable for the multiplexing of RF signals because it is unsuited to prepare wavelengths as many as the number of RBSs. The requirement of the control of laser wavelengths is another drawback of this scheme. WDM is suitable to be

used for purposes such as the duplex of uplink and downlink in radio-on-fiber networks.

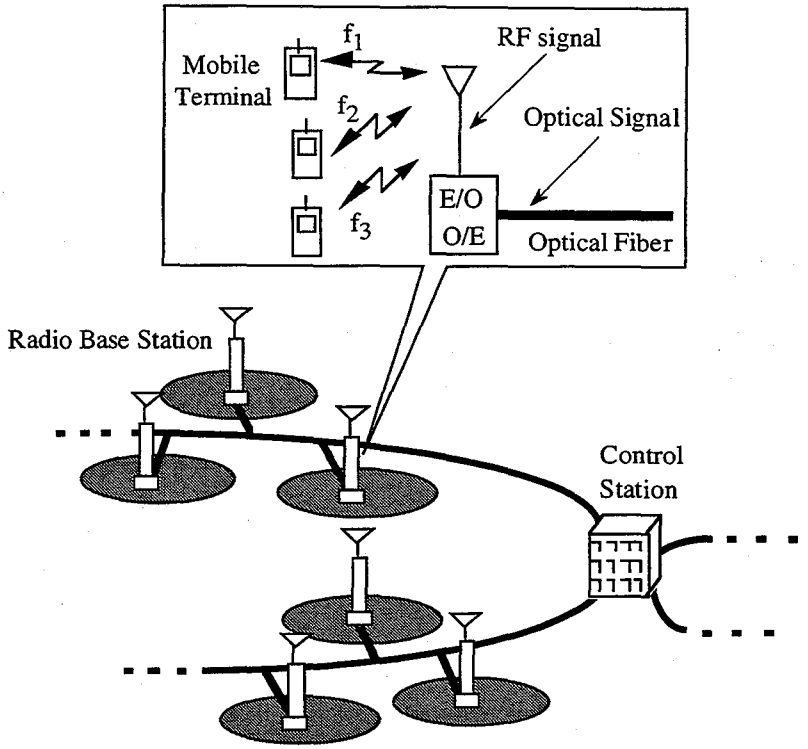

Figure 2.1: Radio-on-Fiber Network.

The SCM scheme has been studied and developed in order to transport multicarrier RF signals over optical fiber in radio-on-fiber systems. Although the optical beat noise occurs if multiple optical sources are used in the SCM systems, and RF signals must be in frequency division multiplexing format, the systems can support such RF signals without the need for any multiplexing equipment. In the SCM system, the optical source or the optical carrier is modulated by RF FDM signals which produce subcarriers of the optical carrier. Each subcarrier can be independently modulated using any conventional modulation format, e.g. FM, AM, FSK, PSK. Thus the optical carrier is capable of supporting multiple channels simultaneously without the need for complicated time, laser wavelength or code division. Another significant characteristic of SCM is that it can be used together with another multiplexing scheme to increase the degree of multiplexing. Therefore, the SCM scheme has been and will still be one of significant multiplexing schemes for radio-on-fiber systems.

Regarding modulation/detection schemes, radio-on-fiber systems using the IM/DD scheme

have been extensively studied because of its simple structure. In IM/DD systems, the optical carrier is intensity-modulated by the RF signal, therefore sidebands with even and odd harmonics are created on both sides of the optical carrier. Owing to fiber chromatic dispersion, relative phase shifts which vary with their wavelengths, fiber distance and modulation frequency are added to these sidebands. At the receiver, each sideband and the optical carrier mix with each other due to square-law detection in a photodiode. At certain relative phases between these components, the beat signals destructively interfere and the output RF signal disappears. By the use of external intensity modulators and ignoring their harmonics outputs, amplitude modulation (AM) and double sideband (DSB) can be achieved. However, IM will be considered as the conventional scheme mainly in this study.

This problem can be solved by dispersion compensation methods such as using chirped fiber Bragg grating (FBG) [51] or an in-line phase conjugator placed in the midst of the optical fiber link [52]. Another approach to overcome the fiber chromatic dispersion problem is the optical single-sideband (SSB) signal transport. The optical SSB signal can be obtained either by optical filtering [23], or optical SSB modulation techniques [12],[30]-[33]. However, the optical filtering method has the disadvantage that half of the optical sideband power is removed which results in 6 dB electrical signal power loss.

As an optical SSB modulation technique, the cascaded phase modulation (CPM) scheme shown in Fig. 2.2 (a) was proposed in Ref. [31]. The concept of the CPM scheme is that a rotating birefringent plate, or a system that simulates the action of such a plate, will act upon a circularly polarized light beam to produce a separable component shifted in frequency. The rotation is accomplished by using Pockels electro-optic effect in a pair of electro-optic crystals such as potassium dihydrogen phosphate (KDP) crystals. Incoming linearly polarized light is passed through a quarter-wave plate (QWP) that functions as a right-handed circular polarizer. The circularly polarized light is passed through two electro-optic crystals along their optical axes. The effect of the rotating birefringent plate is obtained by having the b axes of the two crystals oriented 45 degrees apart, as shown, and applying the modulation voltages in phase quadrature. This concept has also been studied in waveguide configuration as shown in Fig. 2.2 (b) [32],[33]. The voltage $v(t)$ applied to the first phase modulator is orthogonal to the voltage $v'(t)$ applied to the second phase modulator. TE/TM modes and the interference in the waveguide CPM scheme are shown in Fig. 2.3 and Fig. 2.4, respectively. The first phase shifter must be set to $-\pi/4$ ($\phi_1 = -\pi/4$), and the second phase shifter must be set to $+\pi/4$ ($\phi_2 = +\pi/4$) in order to achieve optical SSB modulation in TE mode. In the

waveguide CPM scheme, the pilot carrier is not generated, i.e., this technique is single-sideband suppressed-carrier (SSB-SC) modulation.

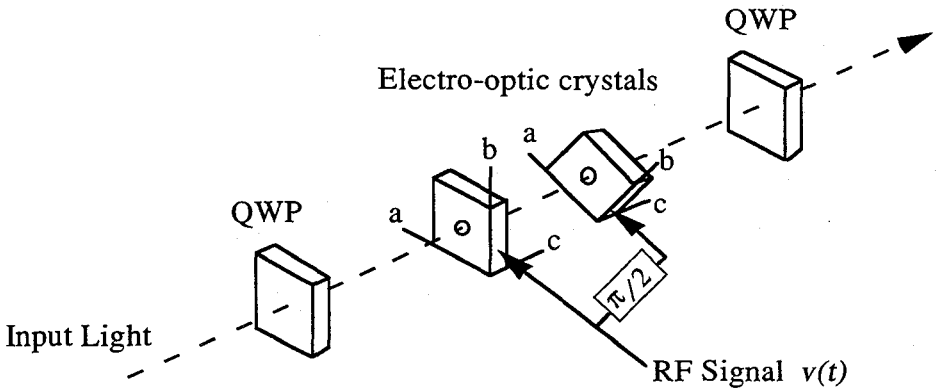

a) Bulk Type

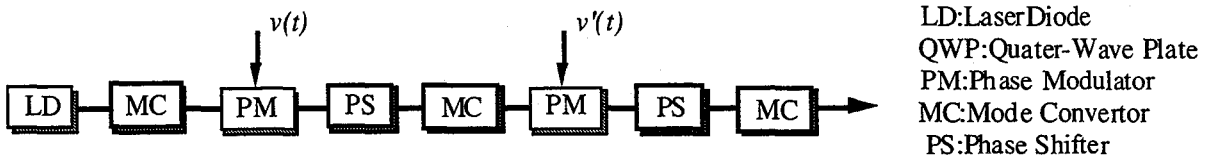

b) Waveguide Type

Figure 2.2: Configuration of the CPM Scheme.

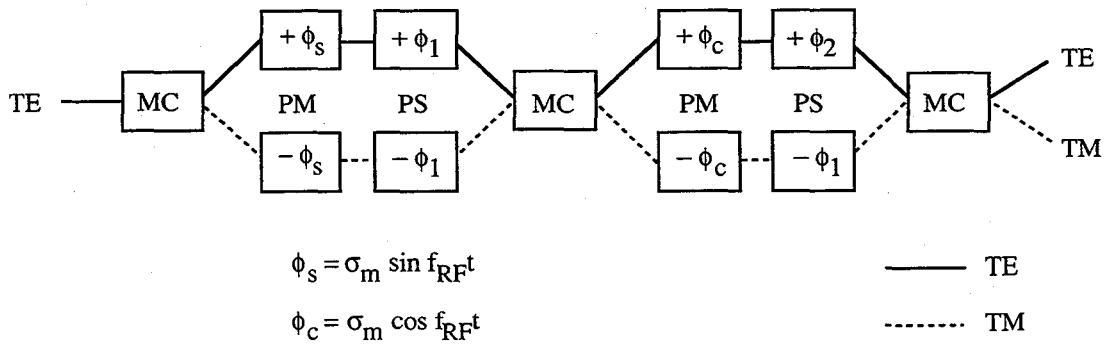

Figure 2.3: TE/TM Modes in the Waveguide CPM Scheme.

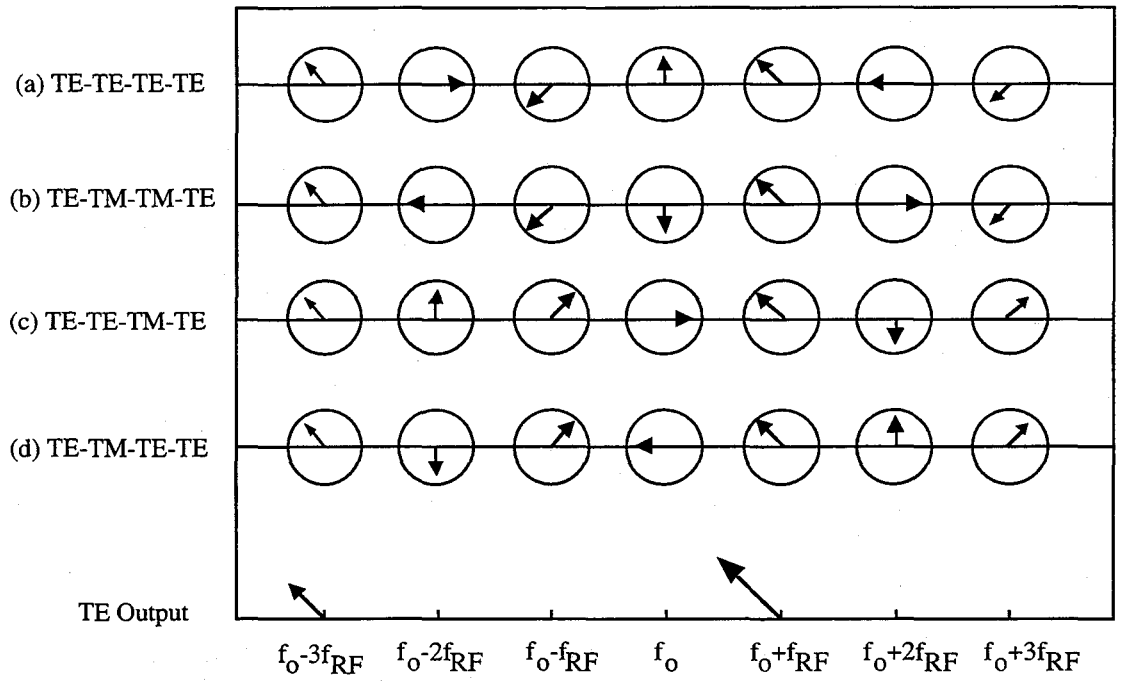

Figure 2.4: Interference in the Waveguide CPM Scheme.

Another type of optical SSB modulator, called a dual Mach-Zehnder (DMZ) interferometer type SSB modulator [30], is shown in Fig. 2.5. Among four outputs of the DMZ scheme, the output $g_2(t)$ contains only single first sideband component and odd order harmonics, and the output $g_3(t)$ has only even order harmonics, because the voltages applied to the phase modulator I and II have polarity inverse to each other (so are the voltages applied to the phase modulator III and IV), and the voltage *v(t)* applied to the phase modulator I and II is orthogonal to the voltage *v'(t)* applied to the phase modulator III and IV. The DMZ scheme is also SSB-SC modulation. The spectrum in each step of the DMZ scheme is shown in Fig. 2.6. In this figure, (a)-(e) are the frequency spectra at the corresponding points in Fig. 2.5.

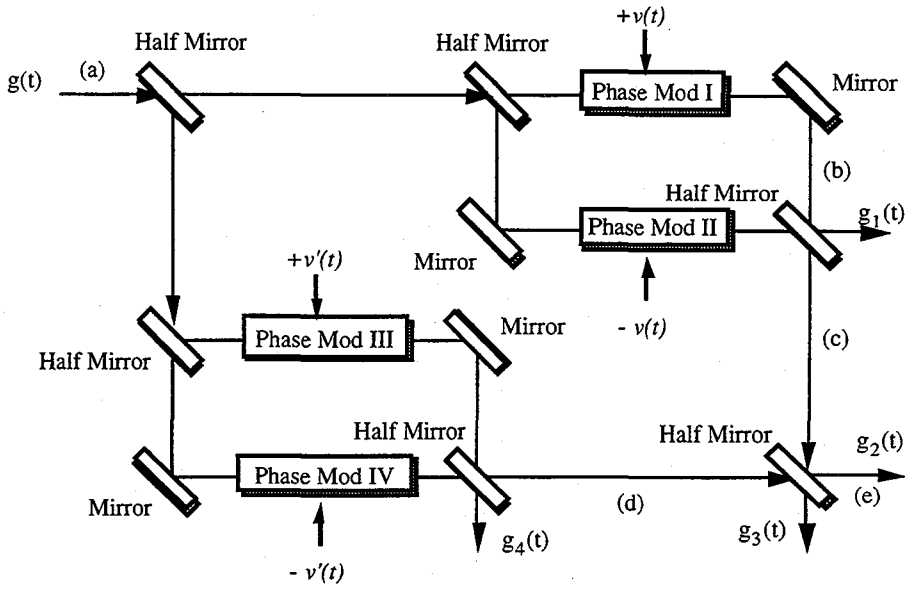

Figure 2.5: Configuration of the DMZ Scheme.

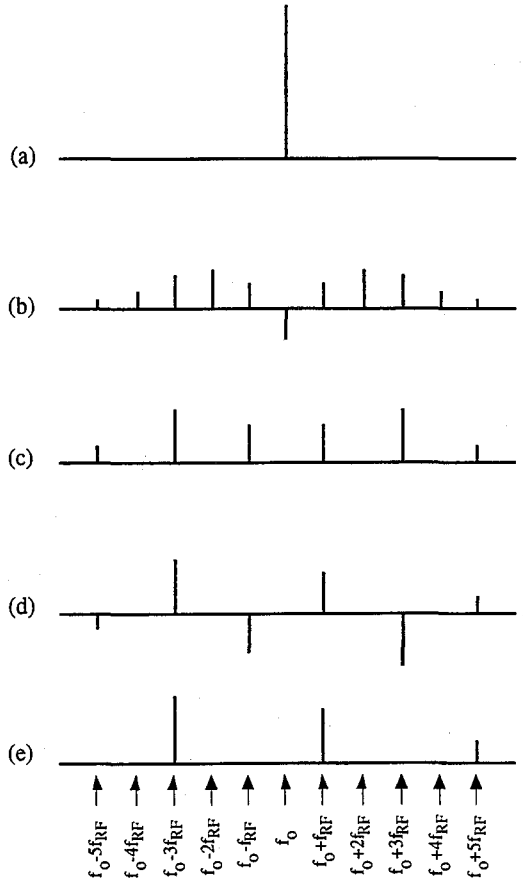

Figure 2.6: Optical Frequency Spectra in the DMZ Scheme.

2.3 Radio-to-Optic Direct Conversion Scheme

2.3.1 Principle of Radio-to-Optic Direct Conversion Scheme

The concept of the ROC scheme, similar to that of the CPM scheme, is that a rotating birefringent plate, or a system that simulates the action of such a plate, will act upon a circularly polarized light beam to produce a separable component shifted in frequency. The difference is, in the ROC scheme, the rotation is accomplished by using Pockels electro-optic effect in a single electro-optic crystal. In other words, in the ROC scheme, the frequency of a light beam is converted with very little loss in intensity by utilizing transverse Pockels effect in a crystal of suitable symmetry. This technique has the advantage that no harmonics are generated and that, except for light losses by reflection or absorption in the crystal, all the incident light can be shifted to the new frequency.

In general the effects of electric field are to rotate the ellipsoid with respect to the crystallographic axis and to change its shape. When the electric fields of the same amplitude and being mutually orthogonal are applied to X and Y axes separately, the ellipsoid is simply rotated about the Z axis of the crystal as shown in Fig. 2.7. The effects of the rotation can transform a left-circularly polarized light beam to produce a right-circularly polarized component at one of the modulation sideband frequencies.

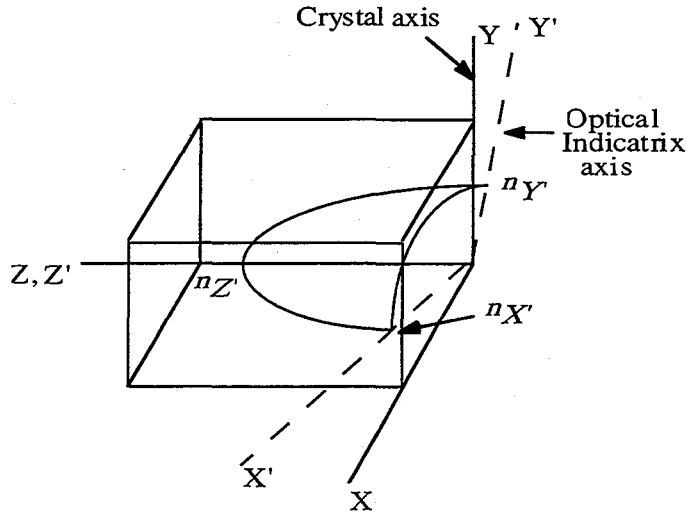

Figure 2.7: Optical Indicatrix Geometry.

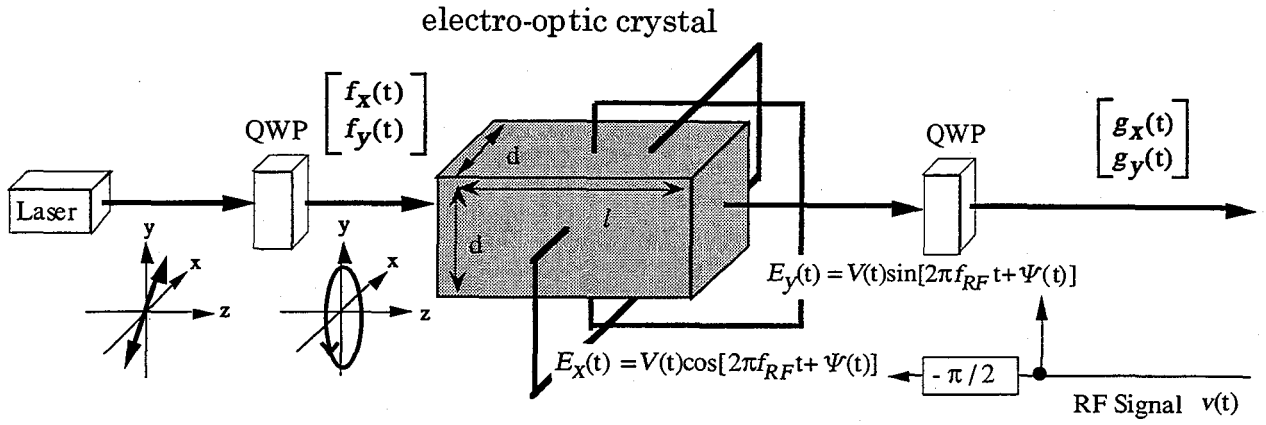

Figure 2.8: Configuration of the ROC Scheme.

A diagram of the radio-to-optic direct converter [21] is shown in Fig. 2.8. Incoming linearly polarized light is passed through the QWP that functions as a right-handed circular polarizer. This circularly polarized light is passed through the electro-optic crystal along its optical axis. At the output of the crystal, the right-handed component rotates in synchronism with the input right-polarized light and can be used as a pilot carrier. On the other hand, the left-handed component experiences one additional left-handed cycle of rotation during each modulation cycle, and therefore the frequency of this component is the sum of the input light frequency and the modulation frequency, i.e., the upper side-band frequency. Finally, both pilot carrier and signal components are linearly polarized by the use of the QWP. The states of polarization of both output components are mutually orthogonal.

2.3.2 Nonlinear Characteristics

In the ROC scheme, when a light propogates along z axis through an electro-optic crystal such as $LiNbO_3$ or $LiTaO_3$, and electric fields, E_x and E_y are applied along the coordinate axes x and y as shown in Fig. 2.4, the equation called the index ellipsoid is given by [53],[54]

$$(\frac{1}{n_o^2} - r_{22}E_y)x^2 + (\frac{1}{n_o^2} + r_{22}E_y)y^2 - r_{22}E_x xy = 1 \qquad (2.1)$$

where r_{ij} and n_o are the electro-optic coefficient and the ordinary refraction index, respectively. Moreover, a new coordinate (X,Y) rotates with respect to coordinate (x,y) by an angle θ, given by

$$\theta = \frac{1}{2}\tan^{-1}\frac{E_x}{E_y} \tag{2.2}$$

The index ellipsoid contains no mixed terms and can be written as

$$\frac{X^2}{n_X^{\,2}} + \frac{Y^2}{n_Y^{\,2}} = 1 \tag{2.3}$$

where n_X and n_Y are the refraction indices along the X and Y axes and can be approximately expressed as

$$n_X \approx n_o\left[1+\frac{1}{2}n_o^{\,2}r_{22}\sqrt{E_x^{\,2}+E_y^{\,2}}\right] \tag{2.4}$$

$$n_Y \approx n_o\left[1-\frac{1}{2}n_o^{\,2}r_{22}\sqrt{E_x^{\,2}+E_y^{\,2}}\right] \tag{2.5}$$

respectively, since in practice the variety of the refraction indices arisen from the electro-optic effect is much smaller than unity. When a light propagates through the crystal along the z axis, its two components polarizing along the X and Y axes receive the phase shifts of ϕ_X and ϕ_Y, given by

$$\phi_X = \frac{2\pi l}{\lambda}n_X \tag{2.6}$$

$$\phi_Y = \frac{2\pi l}{\lambda}n_Y \tag{2.7}$$

where l and λ are the crystal length along the z axis and the light wavelength, respectively. The above operation on the light propagating through the electro-optic crystal is described by a polarization matrix referenced to the x and y axes given by [53]

$$\begin{bmatrix} g_x(t) \\ g_y(t) \end{bmatrix} = \begin{bmatrix} \cos\theta & -\sin\theta \\ \sin\theta & \cos\theta \end{bmatrix} \begin{bmatrix} e^{-j\phi_X} & 0 \\ 0 & e^{-j\phi_Y} \end{bmatrix} \begin{bmatrix} \cos\theta & \sin\theta \\ -\sin\theta & \cos\theta \end{bmatrix} \begin{bmatrix} f_x(t) \\ f_y(t) \end{bmatrix} \tag{2.8}$$

where $f_x(t)$ and $f_y(t)$ are the input optical fields polarized along the x and y axes, and $g_x(t)$ and $g_y(t)$ are the output optical fields. When the driving voltages of the crystal along the x and y axes, $E_x(t)$ and $E_y(t)$, are mutually orthogonal RF signals, i.e.

$$E_x(t) = V(t)\sin(2\pi f_{RF}t + \psi(t)) \tag{2.9}$$

$$E_y(t) = V(t)\cos(2\pi f_{RF}t + \psi(t)) \tag{2.10}$$

where $V(t)$, f_{RF} and $\psi(t)$ are the amplitude, frequency and phase of the RF signal, respectively, and an incident light to the crystal is a right circularly polarized light with a polarization matrix

$$\begin{bmatrix} f_x(t) \\ f_y(t) \end{bmatrix} = \sqrt{P_t}\, e^{j2\pi f_o t} \begin{bmatrix} -j \\ 1 \end{bmatrix} \tag{2.11}$$

where f_o and P_t are the frequency and average intensity of the optical carrier, respectively, the polarization matrix of the output light, $g_x(t)$ and $g_y(t)$ are

$$\begin{aligned} \begin{bmatrix} g_x(t) \\ g_y(t) \end{bmatrix} = & \sqrt{P_t}\cos(\pi\frac{V(t)}{V_\pi}) \cdot e^{j[2\pi f_o t - \phi_o + \phi_s(t)]} \begin{bmatrix} -j \\ 1 \end{bmatrix} \\ & -\sqrt{P_t}\sin(\pi\frac{V(t)}{V_\pi}) \cdot e^{j[2\pi(f_o + f_{RF})t + \psi(t) - \phi_o + \phi_s(t)]} \begin{bmatrix} +j \\ 1 \end{bmatrix} \end{aligned} \tag{2.12}$$

where V_π, ϕ_o, and $\phi_S(t)$ are the half-wave voltage, phase constant, and phase noise of a laser diode, respectively. It is seen from Eq. (2.12) that the output light is composed of two components: one is a right circularly polarized light at the optical carrier frequency f_o , and the other is a left circularly polarized light at the shifted frequency $f_o + f_{RF}$. If the amplitude $V(t)$ is small enough to yield $\pi V(t)/V_\pi << 1$, i.e. $\cos(\pi V(t)/V_\pi) \fallingdotseq 1$ and $\sin(\pi V(t)/V_\pi) \fallingdotseq \pi V(t)/V_\pi$, then the latter component is a replica of the input RF signal in the optical band, with the same amplitude $V(t)$ and phase $\psi(t)$ as the input RF signal. The former can be utilized as a pilot carrier because it has non-modulated amplitude and phase. There are, however, nonlinear distortions in the amplitudes of both the signal component and the pilot carrier component, i.e., $\sin(\pi V(t)/V_\pi)$ and $\cos(\pi V(t)/V_\pi)$, respectively. That is, the amplitude nonlinear distortions vary with the amplitude of the RF signal, $V(t)$. Consequently, only nonlinear distortion in the output amplitude arises and the ROC scheme has a significant merit that no high order sidebands or harmonics are generated. On the other hand, the nonlinear distortions in the IM scheme and conventional optical SSB schemes vary with the instantaneous value of the RF signal, i.e. $V(t)\cos(2\pi f_{RF}t + \psi(t))$.

Owing to the nonlinear distortion, intermodulation distortion occurs in the case of transporting RF subcarrier multiplexing signal, deteriorating the transmission performance. Consequently, it is necessary to examine the performance of the ROC systems in this case. This subject is treated in chapter 3 in detail.

2.4 Concluding Remarks

This chapter addressed the concept of radio-on-fiber networks and the ROC scheme in detail. The multiplexing schemes, the optical IM scheme, and conventional optical SSB modulation schemes were discussed. Also, the nonlinear modulation characteristic of the ROC scheme was described. It can be concluded as follows.

1. In the IM scheme, the power of the output RF signal after detection by the photodiode deteriorates and can be nullified due to the effect of fiber chromatic dispersion.
2. The degradation of the output RF signal due to the effect of fiber chromatic dispersion can be overcome by employing the optical SSB modulation.
3. The ROC scheme, which is one of the optical SSB modulation schemes, has a significant merit over other conventional SSB modulation schemes in that no high order sidebands or harmonics are generated.
4. The above merit of the ROC scheme arises due to the fact that its output amplitude is a nonlinear function of the amplitude of the RF signal, not the function of the instantaneous value. Whereas the nonlinear distortions in conventional IM and SSB schemes are nonlinear function of the instantaneous value of the RF signal.
5. Owing to the nonlinear distortion, intermodulation distortion occurs in the case of transporting RF SCM signal, consequently, the transmission performance deteriorates. Therefore, the transmission performance of the ROC systems in this case has to be examined.

Chapter 3

Subcarrier Multiplexing Radio-to-Optic Direct Conversion Network Systems

3.1 Introduction

In the radio-to-optic direct conversion scheme, there are nonlinear distortions in the amplitudes of both the signal component and the pilot carrier component. These nonlinear distortions vary with the amplitude of the RF signal. Owing to the nonlinear distortions, intermodulation distortions occur in the case of transporting RF subcarrier multiplexing (SCM) signal, consequently, the transmission performance deteriorates. Therefore, this chapter examines the performance of the ROC systems in this case.

The SCM ROC/heterodyne detection (HD) system and the SCM ROC/self-heterodyne detection (SHD) network system are presented in this chapter. In order to evaluate the transmission performance, the received carrier-to-distortion-plus-noise power ratio (CDNR) which is the ratio between the power of received RF subcarrier at a receiver and the power of intermodulation distortion plus noise is theoretically analyzed. The received CDNR of the conventional dual Mach-Zehnder (DMZ) Interferometer type [30] and Cascaded Phase Modulator (CPM) type [31]-[33] optical SSB-suppressed carrier schemes are also theoretically analyzed. The performance improvements by the SCM ROC systems are evaluated by comparing with the conventional SSB modulation and IM systems. The IM system considered here employs direct modulation by a laser diode.

3.2 System Configuration

3.2.1 ROC/Heterodyne Detection System

Figure 3.1 shows the configuration of the ROC/HD system transporting the RF SCM signal. In the RBS, the incoming light is transmitted through the polarization controller in order to match the state of polarization of the light with the axis of the ROC. Then, the RF SCM signal is converted by the ROC into the optical signal with the same modulation format. The pilot carrier component is suppressed by a polarization beam splitter (PBS) and the signal component is transmitted to a CS via optical fiber. At the receiver, after matching the state of polarization of the received light with that of the local oscillator (LO) light by using the polarization controller, heterodyne detection of the received light is achieved by a balanced mixing photodetector. The RF SCM signal is regenerated after passing through a bandpass filter (BPF). In this case, the frequency control and the state of polarization control of the local oscillator can be executed by using feedback of the IF signal.

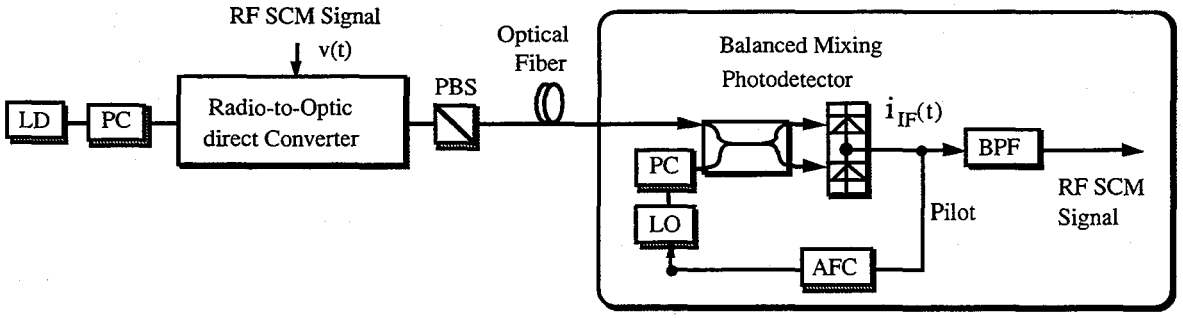

Figure 3.1: SCM ROC/Heterodyne Detection System.

3.2.2 ROC/Self-Heterodyne Detection System

Since the ROC scheme generates a pilot carrier component, self-heterodyne detection (SHD) can be realized. Figure 3.2 shows the configuration of the ROC/SHD system transporting the

RF SCM signal. After the ROC, the pilot carrier component is divided from the signal component by the use of the PBS. The state of polarization of the pilot carrier is matched with that of the signal component by a half-wave plate, and then all the components are combined together by a coupler. At the receiver, the received signal component and the pilot carrier component are self-heterodyne detected by the photodiode. The RF SCM signal is regenerated after passing through the BPF. At the receiver, since the pilot carrier and the signals have resembling phase noises, consequently, some of the phase noises are canceled after detection by the photodiode. The LO, the frequency control, the state of polarization control are not necessary in the ROC/SHD system and the receiver structure becomes simple.

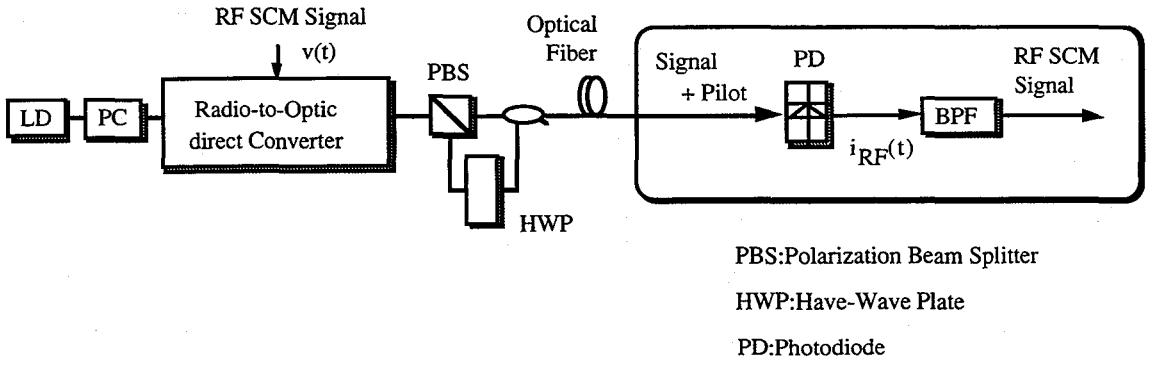

Figure 3.2: SCM ROC/Self-Heterodyne Detection System.

3.3 Theoretical Analysis of Received Carrier-to-Distortion-plus-Noise Ratio (CDNR)

In this section, the received carrier-to-distortion-plus-noise ratios (CDNRs) of the SCM/ROC/HD, SCM/ROC/SHD, SCM/DMZ/HD and SCM/CPM/HD systems are theoretically analyzed.

In this study, we assume that, in all of the four systems, the optical powers of the modulator output are identical (i.e., the transmission optical powers of the RBS are identical), and the propagation losses are also identical. Therefore, the "Received Optical Powers" are the same for all systems.

The "Received Optical Power" is defined in this study as the power of the light received at the receiver, including the modulated optical signals (and, in the case of ROC, the non-

modulated optical carrier signal). In other words, the Received Optical Power is the transmission optical power of the modulator which is deteriorated by the propagation loss between the RBS and the CS.

3.3.1 ROC/Heterodyne Detection System

In the ROC scheme, the N-channel RF SCM signal received at the RBS can be expressed as

$$v(t) = \sum_{k=1}^{N} A_k \cos\left[2\pi(f_{RF} + k\Delta f)t + \theta_k(t)\right] \tag{3.1}$$

where f_{RF} is the frequency of the RF subcarrier. Δf is the frequency interval between adjacent channels. A_k and θ_k are the amplitude and phase of k-th channel RF SCM signal, respectively. The electric fields applied along the coordinate axes x and y of the crystal are given by

$$E_x(t) = \sum_{k=1}^{N} A_k \cos\left[2\pi(f_{RF} + k\Delta f)t + \theta_k(t)\right] \tag{3.2}$$

$$= V(t)\cos\left[2\pi f_{RF}t + \psi(t)\right] \tag{3.3}$$

$$E_y(t) = V(t)\sin\left[2\pi f_{RF}t + \psi(t)\right] \tag{3.4}$$

where $V(t)$ and $\psi(t)$ are the envelope and phase of the RF SCM signal, $v(t)$, respectively, and can be expressed as

$$V(t) = \sqrt{A^2(t) + B^2(t)} \tag{3.5}$$

$$\psi(t) = \tan^{-1}\left(\frac{B(t)}{A(t)}\right) \tag{3.6}$$

where $A(t)$ and $B(t)$ are given by

$$A(t) = \sum_{k=1}^{N} A_k \cos\left[2\pi k\Delta f t + \theta_k(t)\right] \tag{3.7}$$

$$B(t) = \sum_{k=1}^{N} A_k \sin[2\pi k \Delta f t + \theta_k(t)] \tag{3.8}$$

Using Eq. (2.11), the pilot carrier $g_p(t)$ and the signal $g_s(t)$ can be written respectively as

$$g_p(t) = \sqrt{2P_t}\cos(\pi \frac{V(t)}{V_\pi}) \cdot e^{j[2\pi f_o t - \phi_o + \phi_s(t)]} \tag{3.9}$$

$$g_S(t) = \sqrt{2P_t}\sin(\pi \frac{V(t)}{V_\pi}) \cdot e^{j[2\pi(f_o + f_{RF})t - \phi_o + \psi(t) + \phi_s(t)]} \tag{3.10}$$

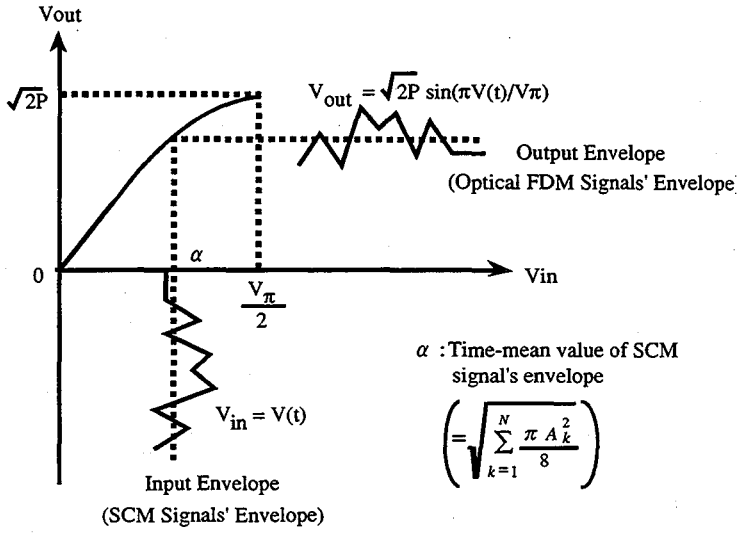

Figure 3.3: Envelope Conversion Characteristic of the ROC Scheme.

Figure 3.3 illustrates the envelope conversion characteristic of ROC. Each amplitude of the subcarrier signal A_k is assumed to be equal to A, and a small optical modulation index (OMI): $m = [\pi\ V(t)/V_\pi] << 1$ is assumed. At the receiver of the ROC/HD system, received optical signals are optically heterodyne-detected with the LO light. The LO light can be expressed as

$$g_L(t) = \sqrt{2P_L}\exp[j\{2\pi(f_o - f_{IF})t + \phi_L(t)\}] \tag{3.11}$$

where P_L and $\phi_L(t)$ are the LO power and the phase noise of the LO light, respectively. Expanding the sinusoidal envelope conversion characteristic by the Taylor expansion with center α (time-mean value of SCM signals' envelope, shown in Fig. 3.3), after the optical heterodyne detection, the signal currents in the IF band are given by

$$i_{IF}(t) = i_p(t) + i_S(t) + i_{IM3}(t) + i_{IM2}(t) \tag{3.12}$$

$$i_p(t) = 2r\sqrt{P_R P_L}\{b_o + b_2 N m^2\}\exp[j\{2\pi f_{IF}t - \phi_o + \Delta\phi(t)] \tag{3.13}$$

$$\begin{aligned} i_S(t) &= 2r\sqrt{P_R P_L}\, m\{a_1 + a_3(2N-1)m^2\} \\ &\cdot \sum_{k=1}^{N} \exp[j\{2\pi(f_{IF} + f_{RF} + k\Delta f)t + \theta_k(t) - \phi_o + \Delta\phi(t)\}] \end{aligned} \tag{3.14}$$

and the 3rd order and 2nd order intermodulation currents can be written as

$$\begin{aligned} i_{IM3}(t) = 2r\sqrt{P_R P_L}\, a_3 m^3 \sum_{h=1}^{N-1} \sum_{\substack{i=h+1 \\ (Condition)}}^{N} \sum_{l=1}^{N} [&\exp[j\{2\pi(f_{IF} + f_{RF} + (i-h+l)\Delta f)t \\ &+ (\theta_i(t) - \theta_h(t) + \theta_l(t)) - \phi_o + \Delta\phi(t)\}] + \exp[j\{2\pi(f_{IF} + f_{RF} \\ &+ (-i+h+l)\Delta f)t + (-\theta_i(t) + \theta_h(t) + \theta_l(t)) - \phi_o + \Delta\phi(t)\}]] \end{aligned} \tag{3.15}$$

$$\begin{aligned} i_{IM2}(t) = 2r\sqrt{P_R P_L}\, a_2 m^2 \sum_{h=1}^{N-1} \sum_{\substack{i=h+1 \\ (Condition)}}^{N} [&\exp[j\{2\pi(f_{IF} + f_{RF} + (i+h)\Delta f)t \\ &+ (\theta_i(t) - \theta_h(t)) - \phi_o + \Delta\phi(t)\}] + \exp[j\{2\pi(f_{IF} + f_{RF} \\ &+ (-i+h)\Delta f)t + (-\theta_i(t) + \theta_h(t)) - \phi_o + \Delta\phi(t)\}]] \end{aligned} \tag{3.16}$$

$$condition: \begin{cases} l \neq h & l > \dfrac{N}{2} \\ l \neq i & l < \dfrac{N}{2} \end{cases}$$

where P_R, r and $\Delta\phi(t)$ are the received optical power including the modulated optical signals and the non-modulated optical carrier signal, the photodetecter responsivity and $\phi_R(t)$-$\phi_L(t)$, respectively. a_k and b_k are given by

$$a_k = \sum_{b=0}^{3-k} \frac{1}{(kb)!}\left(\frac{\pi}{V_\pi}\alpha\right)^k \sin\left(\frac{\pi}{V_\pi} + \frac{\pi}{2}(k+b)\right) \qquad (k = 0,1,2,3) \tag{3.17}$$

$$b_k = \sum_{b=0}^{3-k} \frac{1}{(kb)!}\left(\frac{\pi}{V_\pi}\alpha\right)^k \cos\left(\frac{\pi}{V_\pi} + \frac{\pi}{2}(k+b)\right) \qquad (k = 0,1,2,3) \tag{3.18}$$

Figure 3.4 illustrates the power spectrum density in the IF band. It can be seen that the second order intermodulation distortion (IM2) falls in the signal band as well as the third order intermodulation distortion (IM3). This phenomenon, which is different from that in other conventional schemes, is due to the fact that the nonlinear modulation characteristics in the ROC scheme varies with an envelope of the RF SCM signal, as shown in Eq. (3.9) and (3.10), whereas it varies with an instantaneous value of the RF SCM signal in other schemes. Consequently, IM2 and IM3 in the ROC scheme (as shown in Eq. (3.16) and Eq. (3.15), respectively) are different from those in other schemes. The carrier power per subcarrier channel can be expressed as

$$P_{HD} = 2r^2 P_R P_L \{a_1 m + a_3(2N-1)m^3\}^2 \tag{3.19}$$

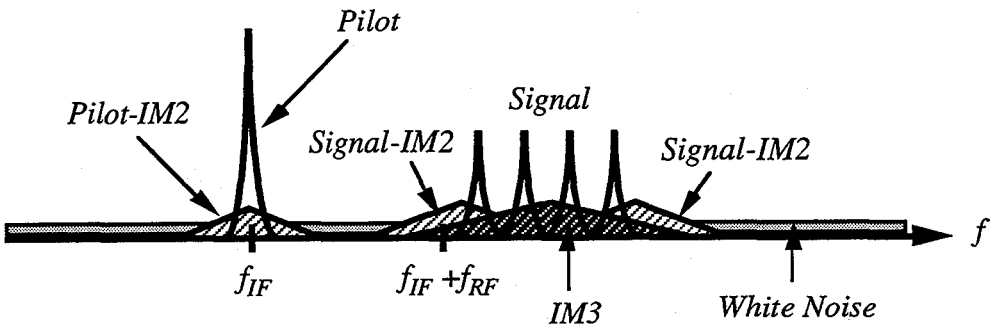

Figure 3.4: Power Spectrum Density in the IF Band in the ROC/HD System.

Considering at the central channel of the SCM channels where the largest IM3 occurs, the IM3 power, σ^2_{IM3}, is given by

$$\sigma^2_{IM3} = 2r^2 P_R P_L D_3 a_3^2 m^6 \tag{3.20}$$

where D_3 is the number of IM3 dropping in the central channel, which can be written as

$$D_3 = \begin{cases} \frac{1}{4}(N-1)(3N-5) & N: odd \\ \frac{1}{4}(N-1)(3N-2) & N: even \end{cases} \tag{3.21}$$

Figure 3.5 shows the relationship between the power of one IM2, P_{IM2}, the power of one IM3, P_{IM3}, which drop in the signal band and the optical modulation index, m, in the case that the radio channel number N is 3 or 100. It is found from the figure that as the optical modulation index increases, both P_{IM3} and P_{IM2} increase. Also, as number of radio channels becomes larger, P_{IM2} increases, while P_{IM3} is almost unchanged. It can be concluded that IM3 dominates over IM2, because the ROC is used at small m and the number of IM3 dropping in the signal band is much larger than that of IM2.

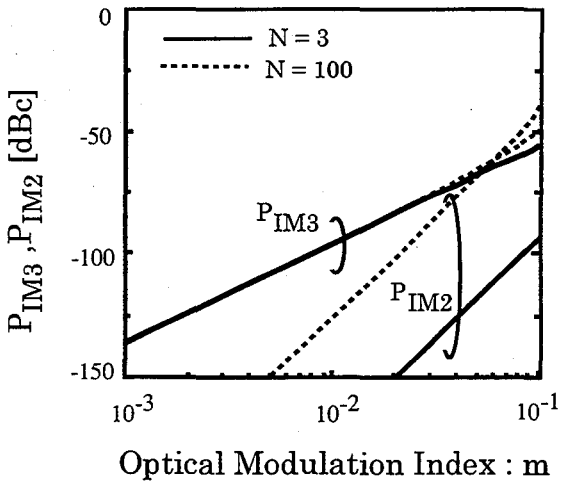

Figure 3.5: Power of IM2 and IM3 in the ROC/HD System.

The noises considered here are the signal and LO shot noises, the receiver thermal noise, and the relative intensity noise (RIN) of which powers are given respectively by

$$\sigma^2_{sh} = 2er(P_L + P_R)B \tag{3.22}$$

$$\sigma^2_{th} = \frac{8kT}{R_L}B \tag{3.23}$$

$$\sigma^2_{rin} = RIN\, r^2 P_R P_L B \tag{3.24}$$

where e, k, T, R_L, B, and RIN are the, electron charge, Boltzmann constant, noise temperature, load resistance, signal bandwidth, and relative intensity noise, respectively. Hence, the total noise power, σ^2_n, can be expressed as

$$\sigma^2_n = \sigma^2_{sh} + \sigma^2_{th} + \sigma^2_{rin} \tag{3.25}$$

Therefore, the received CDNR of the ROC/HD system is given by

$$CDNR = \frac{2r^2 P_R P_L \{a_1 m + a_3(2N-1)m^3\}^2}{2r^2 P_R P_L D_3 a_3{}^2 m^6 + \sigma_n{}^2} \tag{3.26}$$

3.3.2 ROC/Self-Heterodyne Detection System

In the ROC/SHD system, after direct detection by the photodiode, the output currents are composed of the product of the signal and the pilot carrier, $i_{S\text{-}P}(t)$, the product of the pilot carrier and the signal IM3, $i_{IM3\text{-}P}(t)$, the product of the signal and the pilot IM2, $i_{IM2\text{-}S}(t)$, and the noise, $n(t)$, which can be written as

$$i_{S-P}(t) = 2rP_R m\{a_o + a_3(2N-1)m^2\}\{b_o + b_2 N m^2\}\sum_{k=1}^{N}\exp[j\{2\pi(f_{RF} + k\Delta f)t + \psi(t)\}] \tag{3.27}$$

$$\begin{aligned} i_{IM3-P}(t) = 2rP_R a_3 m^3\{b_o + b_2 N m^2\}\sum_{h=1}^{N-1}\sum_{\substack{i=h+1 \\ (Condition)}}^{N}\sum_{l=1}^{N}[\exp[j\{2\pi(f_{RF} + (i-h+l)\Delta f)t \\ + (\theta_i(t) - \theta_h(t) + \theta_l(t))\}] + \exp[j\{2\pi(f_{RF} + (-i+h+l)\Delta f)t + \\ (-\theta_i(t) + \theta_h(t) + \theta_l(t))\}]] \end{aligned} \tag{3.28}$$

$$\begin{aligned} i_{IM2-S}(t) = 2rP_R b_2 m^2\{a_o + a_3(2N-1)m^2\}\sum_{h=1}^{N-1}\sum_{\substack{i=h+1 \\ (Condition)}}^{N}\sum_{l=1}^{N}[\exp[j\{2\pi(f_{RF} + (i-h+l)\Delta f)t \\ + (\theta_i(t) - \theta_h(t) + \theta_l(t))\}] + \exp[j\{2\pi(f_{RF} + (-i+h+l)\Delta f)t + \\ (-\theta_i(t) + \theta_h(t) + \theta_l(t))\}]] \end{aligned} \tag{3.29}$$

Figure 3.6 illustrates the power spectrum density of ROC/SHD system in RF band. The carrier power per subcarrier channel can be expressed as

$$P_{SHD} = 2r^2 P_R^2 \{a_1 m + a_3(2N-1)m^3\}^2 \cdot \{b_o + b_2 N m^2\}^2 \tag{3.30}$$

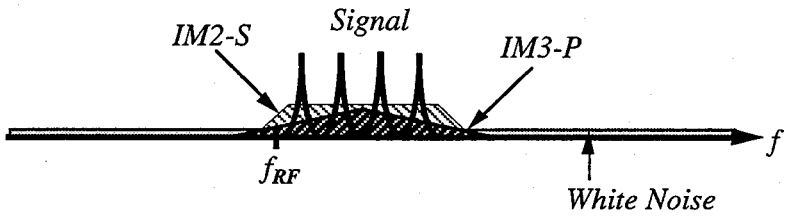

Figure 3.6: Power Spectrum Density in the RF Band in the ROC/SHD System.

Using the same assumptions as the analysis for ROC/HD system, the power of $i_{IM3\text{-}P}(t)$, $\sigma^2_{IM3\text{-}P}$, and the power of $i_{IM2\text{-}S}(t)$, $\sigma^2_{IM2\text{-}S}$, are respectively given by

$$\sigma^2{}_{IM3-P} = 2r^2 P_R^2 D_3 a_3^2 m^6 \{b_o + b_2 N m^2\}^2 \tag{3.31}$$

$$\sigma^2{}_{IM2-S} = 2r^2 P_R^2 D_2' b_2^2 m^4 \{a_1 + a_3(2N-1)m^2\}^2 \tag{3.32}$$

where D'_2 is the number of the pilot IM2 dropping in the central channel, which can be written as

$$D_2' = \begin{cases} \frac{1}{4}(N-1)(3N-1) & N: odd \\ \frac{1}{4}N(3N-4) & N: even \end{cases} \tag{3.33}$$

In ROC/SHD system, the signal shot noise, the receiver thermal noise, and the RIN are given by

$$\sigma'^2{}_{sh} = 2erP_R B \tag{3.34}$$

$$\sigma'^2_{th} = \frac{4kT}{R_L} B \tag{3.35}$$

$$\sigma'^2_{rin} = RIN\, r^2 P_R^2 B \tag{3.36}$$

Hence, the total noise power, σ'^2_n, and the received CDNR of the ROC/SHD system can be expressed respectively as

$$\sigma'^2_n = \sigma'^2_{sh} + \sigma'^2_{th} + \sigma'^2_{rin} \tag{3.37}$$

$$CDNR = \frac{2r^2 P_R^2 \{a_1 m + a_3(2N-1)m^3\}^2 \cdot \{b_o + b_2 N m^2\}^2}{\sigma^2_{IM3-P} + \sigma^2_{IM2-S} + \sigma'^2_n} \tag{3.38}$$

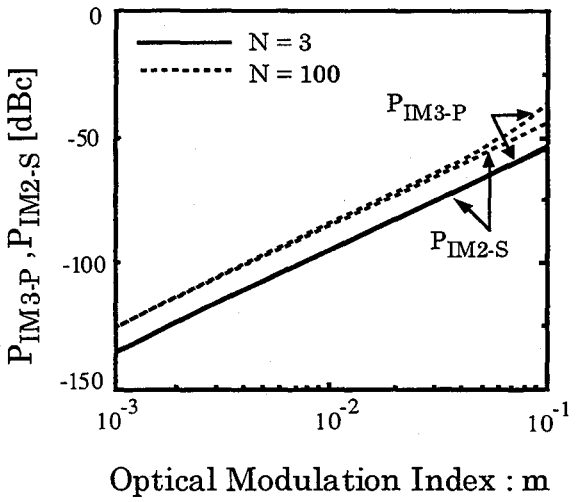

Figure 3.7: Power of IM3-P and IM2-S in the ROC/SHD System.

In the ROC/SHD system, the pilot IM2 dominates the received CDNR performance as much as the IM3. The considerable intermodulation distortions arising at the photodetector output, are the product of IM3 and the pilot carrier (IM3-P), and the product of the signal and the pilot IM2 (IM2-S). Figure 3.7 shows the power of IM2-S, $P_{IM2\text{-}S}$, and the power of IM3-P, $P_{IM3\text{-}P}$, as a function of the optical modulation index, m, in the case that the number of radio channels is 3 or 100. As the optical modulation index increases or as the number of radio channels increases, both $P_{IM2\text{-}S}$ and $P_{IM3\text{-}P}$ increase. Furthermore, the $P_{IM2\text{-}S}$ is almost the same as $P_{IM3\text{-}P}$.

3.3.3 Dual Mach-Zehnder/Heterodyne Detection System

The N-channel RF SCM signal received at the RBS can be expressed as Eq.(3.1). In the DMZ/HD system, after optical heterodyne detection, the output current can be written as

$$\begin{aligned} i_{DMZ}(t) = r\sqrt{\frac{P_L P_R}{8}}[j\exp[j\{2\pi f_{IF}t + \frac{\pi}{V_\pi}v(t)\}] - j\exp[j\{2\pi f_{IF}t - \frac{\pi}{V_\pi}v(t)\}] \\ + \exp[j\{2\pi f_{IF}t - \frac{\pi}{V_\pi}v'(t)\}] - \exp[j\{2\pi f_{IF}t + \frac{\pi}{V_\pi}v'(t)\}]] + n(t) \end{aligned} \tag{3.39}$$

where the radio signal $v'(t)$ is

$$v'(t) = \sum_{k=1}^{N} A_k \sin\{2\pi(f_{RF} + k\Delta f)t + \theta_k(t)\} \tag{3.40}$$

Here, we assume that the modulation indices of all four phase modulators are small and equal to γ. Expanding the output current by the 1st kind of Bessel function and ignoring higher order other than -1,0 and 1, the IF current can be expressed as

$$i_{IF-DMZ}(t) = \sum_{k=1}^{N} i_{S_{k-DMZ}}(t) + \sum_{k=1}^{N} i_{IM3_{k-DMZ}}(t) + n(t) \tag{3.41}$$

where $i_{S_{k-DMZ}}(t)$ and $i_{IM3_{k-DMZ}}(t)$ are the regenerated radio signal and the IM3 current, given respectively by

$$i_{S_{k-DMZ}}(t) = 2r\sqrt{P_L P_R}[J_o(\gamma)]^{N-1}[J_1(\gamma)]\exp[j\{2\pi(f_{IF} + f_{RF} + k\Delta f)t + \theta_k(t) + \frac{\pi}{2}\}] \tag{3.42}$$

$$\begin{aligned} i_{IM3_{k-DMZ}}(t) = 2r\sqrt{P_L P_R}[J_o(\gamma)]^{N-3}[J_1(\gamma)]^2[J_{-1}(\gamma)]K_3\exp[j\{2\pi\{f_{IF} + (f_{RF} + h\Delta f) \\ + (f_{RF} + i\Delta f) - (f_{RF} + l\Delta f)\}t + (\theta_h(t) + \theta_i(t) - \theta_l(t)) + \frac{\pi}{2}]] \end{aligned} \tag{3.43}$$

where K_3 is the number of the IM3 dropping in the central channel, given by

$$K_3 = \begin{cases} \frac{1}{8}(N+1)^2 + \frac{1}{4}\{(N-13)^3 - 5\} - \frac{1}{8}\{1-(-1)^N\}(-1)^{\frac{(3N+1)}{2}} & N: odd \\ \frac{1}{8}N(N+1) + \frac{1}{4}\{(N-13)^3 - 5\} - \frac{1}{8}\{1-(-1)^N\}(-1)^{\frac{3N}{2}} & N: even \end{cases} \quad (3.44)$$

Figure 3.8 illustrates the power spectrum density of the DMZ/HD system in the IF band. Considering at the central channel of SCM channels, the carrier power per subcarrier channel can be written as

$$P_{DMZ} = 2r^2 P_L P_R [J_o(\gamma)]^{2N-2} [J_1(\gamma)]^2 \quad (3.45)$$

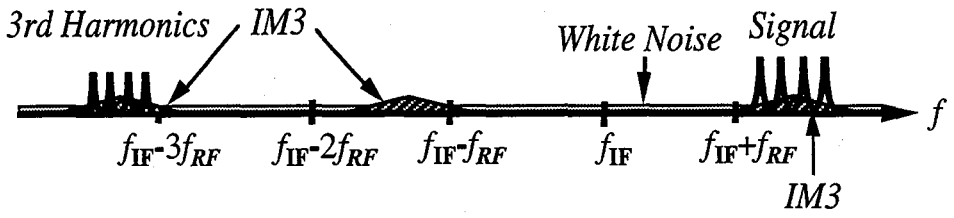

Figure 3.8: Power Spectrum Density in the IF Band in the DMZ/HD System.

The power of the IM3 and the noise power are given by

$$\sigma^2_{IM3-DMZ} = 2r^2 P_L P_R [J_o(\gamma)]^{2N-6} [J_1(\gamma)]^4 [J_{-1}(\gamma)]^2 K_3 \quad (3.46)$$

$$\sigma^2_{n-DMZ} = \{RINr^2 P_L P_R + 2er(P_L + P_R) + \frac{8k_B T}{R_L}\}B \quad (3.47)$$

Therefore, the received CDNR of the DMZ/HD system can be expressed as

$$CDNR = \frac{P_{DMZ}}{\sigma^2_{IM3-DMZ} + \sigma^2_{n-DMZ}} \quad (3.48)$$

3.3.4 Cascaded Phase Modulation/Heterodyne Detection System

In the CPM/HD system, after optical heterodyne detection, the output current is given by

$$\begin{aligned} i_{CPM}(t) = r\sqrt{\frac{P_L P_R}{2}}[&\exp[j\{2\pi f_{IF}t + \frac{\pi}{\sqrt{2}V_\pi}v(t)\}] - j\exp[j\{2\pi f_{IF}t - \frac{\pi}{\sqrt{2}V_\pi}v(t)\}] \\ + \; &j\exp[j\{2\pi f_{IF}t + \frac{\pi}{\sqrt{2}V_\pi}v'(t)\}] - \exp[j\{2\pi f_{IF}t - \frac{\pi}{\sqrt{2}V_\pi}v'(t)\}]] + n(t) \end{aligned} \tag{3.49}$$

where *v(t)* and *v'(t)* are the same as those of DMZ/HD system. Here, we assume that the modulation indices of the cascaded two phase modulators are small and equal to β. The current in the IF band may be written as

$$i_{IF-CPM}(t) = \sum_{k=1}^{N} i_{S_{k-CPM}}(t) + \sum_{k=1}^{N} i_{IM3_{k-CPM}}(t) + n(t) \tag{3.50}$$

where $i_{S_{k-CPM}}(t)$ and $i_{IM3_{k-CPM}}(t)$ are the subcarrier signal and the IM3 current, respectively, and given by

$$i_{S_{k-CPM}}(t) = 2r\sqrt{2P_L P_R}[J_o(\beta)]^{N-1}[J_1(\beta)]\exp[j\{2\pi(f_{IF} + f_{RF} + k\Delta f)t + \theta_k(t) + \frac{\pi}{2}\}] \tag{3.51}$$

$$\begin{aligned} i_{IM3_{k-CPM}}(t) = 2r\sqrt{2P_L P_R}[J_o(\beta)]^{N-3}&[J_1(\beta)]^2[J_{-1}(\beta)]K_3\exp[j\{2\pi\{f_{IF} + (f_{RF} + h\Delta f) \\ &+ (f_{RF} + i\Delta f) - (f_{RF} + l\Delta f)\}t + (\theta_h(t) + \theta_i(t) - \theta_l(t)) + \frac{\pi}{2}]] \end{aligned} \tag{3.52}$$

Hence, the power spectrum density in the IF band is the same as that of the DMZ/HD system (Figure 3.9). At the central channel of the SCM channels, the carrier power per subcarrier channel can be expressed as

$$P_{CPM} = 4r^2 P_L P_R [J_o(\beta)]^{2N-2}[J_1(\beta)]^2 \tag{3.53}$$

and the power of the IM3 may be written as

$$\sigma^2_{IM3-CPM} = 4r^2 P_L P_R [J_o(\beta)]^{2N-6} [J_1(\beta)]^4 [J_{-1}(\beta)]^2 K_3 \quad (3.54)$$

Since the noises in this system are the same as those of SCM/DMZ/HD system (Eq. (3.47)), the received CDNR of the CPM/HD system is given by

$$CDNR_{CPM} = \frac{P_{CPM}}{\sigma^2_{IM3-CPM} + \sigma^2_{n-CPM}} \quad (3.55)$$

3.4 Numerical Results and Discussions

In this section, we show some numerical results of CDNR of the ROC and conventional systems and also discuss. Table 1 shows the parameters used in calculations. Here, we choose the optimum optical modulation index for the ROC systems, the optimum optical phase modulation indices for DMZ and CPM systems to maximize the CDNR.

Table 1 Parameters used in calculations

Local Light Power: P_L	10 dBm
Relative Intensity Noise: RIN	-152 dB/Hz
Photodiode: r	0.8 A/W
Load Resistance: R_L	50 Ω
Noise Temperature: T	300 K

3.4.1 Carrier-to-Distortion-plus-Noise Ratio

In this study, it is assumed that the optical powers of the modulator output and the propagation losses are identical in all systems. Therefore, the received optical powers are the same for all systems.

Figure 3.9 shows the relationship between the received CDNR and the received optical power of the ROC/HD, DMZ/HD and CPM/HD systems in the case of the number of channels N of 20 and the radio signal bandwidth per channel of 150 MHz. The CDNR performance of the ROC/SHD system and the IM/DD system are also shown. For the IM/DD

system, the 3rd order laser diode nonlinear coefficient, c_3, is assumed to be 0.01. In the case of very small received optical power, the CDNR of ROC system is inferior compared with DMZ and CPM system, because the optical modulation index, m, of the ROC system is limited to $\pi/2$, therefore the carrier power is limited. On the other hand, for the received power of more than about -45 dBm, the ROC/HD system presents the highest CDNR performance among three HD systems. This is because the ROC scheme can allocate the optical power solely to the RF SCM signal component, that is the first order component, whereas in both DMZ and CPM schemes, some optical power is used in the third order and higher order harmonics. It is also seen from Eq. (3.26), (3.48) and (3.55) that ROC can improve CDNR of DMZ and CPM by about 5 dB and 2.5 dB, respectively. After heterodyne

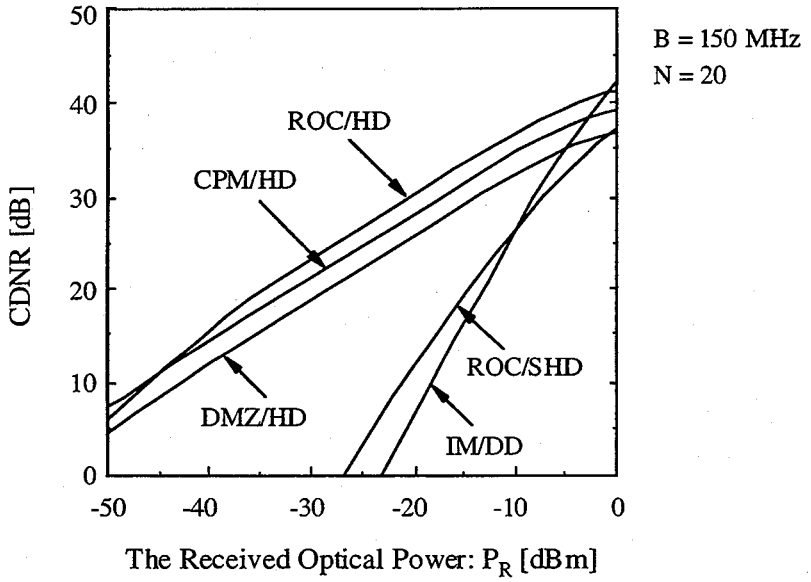

Figure 3.9 Relationship between the Received CDNR and the Received Optical Power.

detection, the carrier power per subcarrier channel in CPM system (Eq. (3.55)) is larger than that in DMZ system (Eq. (3.48)) because the powers used in 3rd order and higher order harmonics in DMZ system are larger than those in CPM system. Comparing ROC/SHD system with IM/DD system (see Appendix A), the ROC/SHD system can improve the CDNR of IM/DD system by about 5 dB for the received optical power of less than -10 dBm. This is due to the fact that the received RF power of the ROC/SHD system is larger than that of the IM/DD system, and in this region, the power of the intermodulation

distortion which depends on the received optical power is small. Consequently, the effect of the intermodulation distortion which is larger in the ROC/SHD system than in the IM/DD system (as shown in Fig. 3.11) diminishes.

Figures 3.10 shows the CDNR versus the number of channels N for the ROC/HD, DMZ/HD and CPM/HD systems in the case of the RF signal bandwidth per channel of 150 MHz and the received optical power P_R of -10dBm. For comparison, the CDNR of the conventional AM/HD system [55],[56] is also shown. For ROC, DMZ and CPM systems, CDNR decreases due to increasing IM3 distortion power as N increases. On the other hand, in the case of the number of channels of more than 20, IM2 distortion power deteriorates CDNR of AM/HD system severely, because the frequency arrangement in SCM channels turns into multi-octave in this region of number of channels. However, since the ROC, DMZ

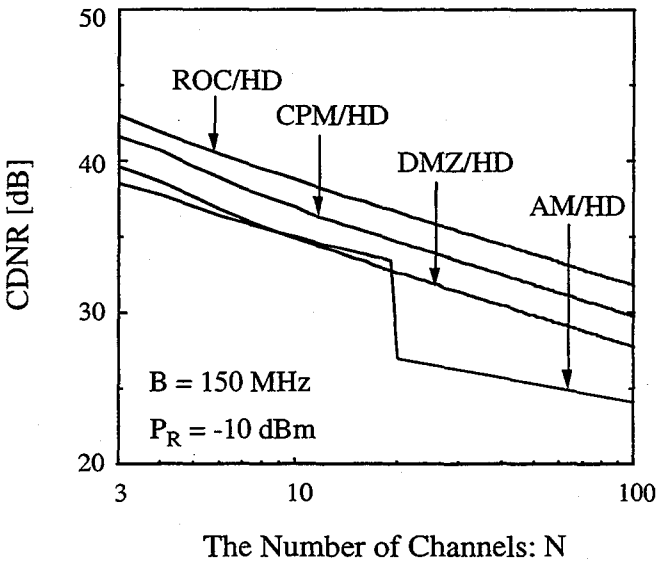

Figure 3.10: Relationship between the Received CDNR and the Number of Channels of the RF SCM Signal.

and CPM systems do not generate any 2nd order harmonics and intermodulation components (IM2), CDNR moderately decreases according to number of channels. Hence, for SCM coherent radio-over-fiber system, ROC system and the SSB using DMZ or CPM system can provide a larger transmission capacity than the conventional SCM AM or IM system. If we assume that the transmission optical powers of the laser diode are identical for all of the three systems, we may expect that ROC system would have an even better

improvement in the CDNR over DMZ and CPM systems, because there is no coupling loss in ROC system.

3.4.2 Spurious-Free Dynamic Range

In this subsection, we discuss the spurious-free dynamic range characteristics of the ROC systems and conventional systems. The dynamic range is one of the important measures of analog link performance, defined as the ratio of the largest signal the system can transport to the smallest. Due to system nonlinearities, spurious intermodulation products are created that can mask or mimic real signals. Therefore, the spurious-free dynamic range (SFDR) is often used as a measure of system performance. The SFDR is the dynamic range where the maximum signal level is limited by the intermodulation products. In other words, it is defined as the range of RF input powers for which the RF input signal can be clearly distinguished from noise and nonlinearities at the link output.

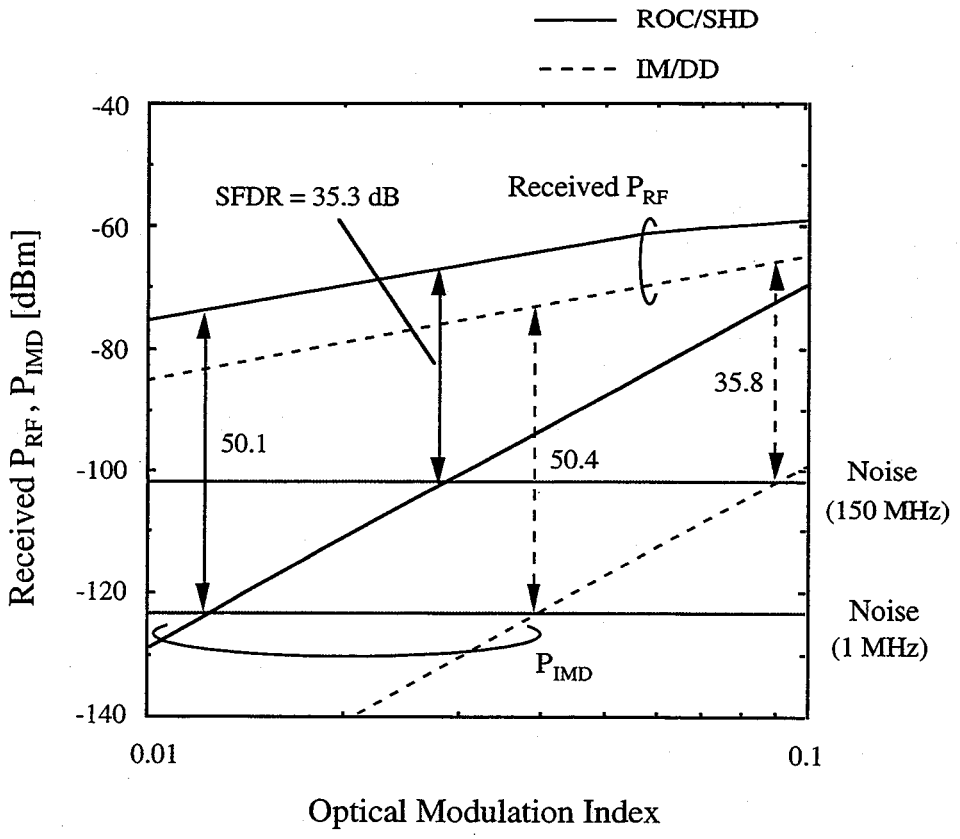

Figure 3.11: SFDR of the ROC/SHD and IM/DD Systems.

Figures 3.11 shows the received RF power and intermodulation distortion power versus the normalized OMI for the ROC/SHD and IM/DD systems in the case of the received optical power P_R of -5 dBm and the number of channels N of 20. The SFDR of each system can be determined as shown in the figure. The SFDRs of the ROC/SHD system are 35.3 dB and 50.1 dB in the case of signal bandwidth of 150 MHz and 1 MHz, respectively. The SFDRs of the ROC/SHD system are approximately the same as those of the IM/DD system. This is because, although the received RF power of the ROC/SHD system is larger than that of the IM/DD system, but the intermodulation distortion power of the ROC/SHD system is larger than that of IM/DD system due to the effect of the pilot IM2.

Recently, the required dynamic range for PCS is being greatly reduced by using CDMA, which is robust against noise and distortion [57]. Furthermore, the fluctuation in received radio signals at the antenna port is very small because of the tight power control of mobile terminals. As a result, the required dynamic range may be considered to be approximately 40 dB. The systems with lower SFDR can be applied to outdoor radio-on-fiber systems with no obstruction or indoor radio-on-fiber systems such as a wireless local area network (wireless LAN) system.

Figures 3.12 shows the received RF power and IM3 power versus the normalized OMI for ROC/HD, CPM/HD and DMZ/HD systems in the case of the received optical power P_R of -5 dBm and the number of channels N of 20. The SFDRs of the ROC/HD system are 42.1 dB and 56.8 dB in the case of signal bandwidth of 150 MHz and 1 MHz, respectively. These SFDRs are approximately 2 dB and 4 dB improved over CPM/HD and DMZ/HD systems, respectively.

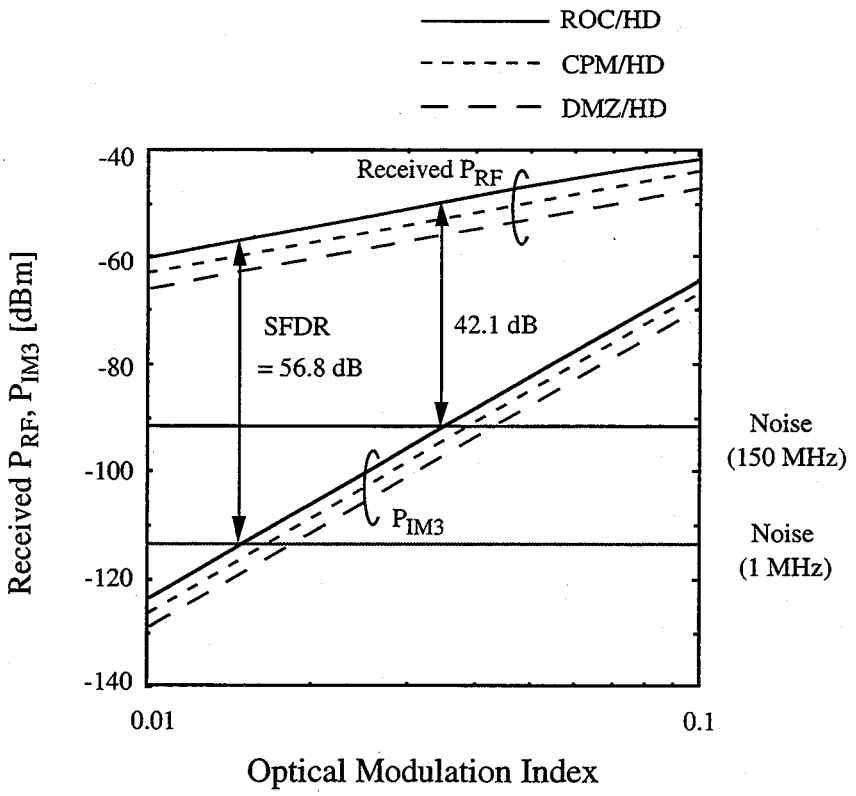

Figure 3.12: SFDR of the ROC/HD, CPM/HD, and DMZ/HD Systems.

3.5 Concluding Remarks

This chapter proposed the ROC/HD and ROC/SHD systems for SCM coherent radio-on-fiber systems and theoretically analyzed the received CDNR taking into account the effect of intermodulation distortion. The received CDNR performance and SFDR performance of the ROC/HD and ROC/SHD systems were discussed and compared with the conventional DMZ/HD, CPM/HD and IM/DD systems. Following results were found:

1. The received CDNR of the ROC/HD system is approximately 5 dB and 2.5 dB better than those of the DMZ/HD and CPM/HD systems, respectively, for every number of channels. This is because the ROC scheme can allocate the optical power to the 1st order component solely, while in both of the DMZ and CPM schemes, some optical power is used in the 3rd order and higher order harmonics.

2. In the case of multi-octave RF SCM signal, the ROC, DMZ and CPM systems are not affected by the 2nd order intermodulation distortion, and can remarkably improve the received CDNR over the conventional AM/HD and IM/DD systems.

3. The ROC/SHD system can improve the received CDNR performance over the IM/DD system by about 5 dB for the received optical power of less than -10 dBm. This is because the received RF power of the ROC/SHD system is larger than that of the IM/DD system, and in this region, the power of the intermodulation distortion which depends on the received optical power is small, consequently, the effect of the intermodulation distortion which is larger in the ROC/SHD system than in the IM/DD system diminishes.

4. The SFDRs the ROC/HD system are 42.1 dB and 56.8 dB in the case of the received optical power of -5 dBm and the number of channels of 20, for the signal bandwidth of 150 MHz and 1 MHz, respectively. These SFDRs are approximately 2 dB and 4 dB improved over those of the CPM/HD and DMZ/HD systems, respectively.

5. The SFDRs the ROC/SHD system are 35.3 dB and 50.1 dB in the case of the received optical power of -5 dBm and the number of channels of 20, for the signal bandwidth of

150 MHz and 1 MHz, respectively. The SFDR of the ROC/SHD system is approximately the same as that of the IM/DD system whose 3rd order laser diode nonlinear coefficient is 0.01. This is because, although the received RF power of the ROC/SHD system is larger than that of the IM/DD system, but the intermodulation distortion power of the ROC/SHD system is larger than that of the IM/DD system due to the existence of the pilot IM2.

Chapter 4

Cascaded Radio-to-Optic Direct Conversion Network Systems

4.1 Introduction

In the uplink of radio-on-fiber systems employing star-type link [34],[35] and bus-type link [36],[37], performance degradation due to beat noise is a severe issue [58]-[60]. Since optical signals from individual optical transmitters are simultaneously transmitted in the network, beat noise arises in the optical receiving process if the optical spectra of these signals overlap. This beat noise seriously degrades the carrier-to-noise ratio (CNR) performance. Therefore, it is necessary to control the wavelength spacing of laser diodes [59] or to use low-coherency light sources, such as light emission diodes (LEDs) or superluminescent diodes (SLDs) [58]. Wavelength division multiplexing (WDM) technique can solve this problem, however, this technique requires complicated control of wavelengths of the laser.

Another solution to this problem is to employ a cascade-type link. The cascaded IM/DD scheme and cascaded phase modulation (PM)/HD scheme have been proposed and studied [38],[39]. However, transmission performance of the conventional cascade-type link systems

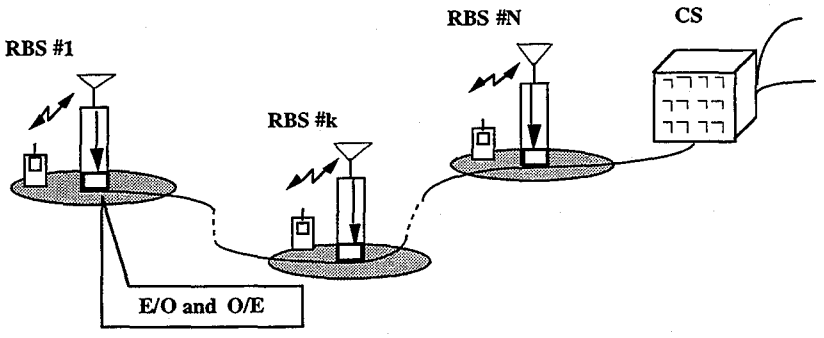

Figure 4.1: Cascaded Radio-on-Fiber Network.

suffers severely from the intermodulation distortion even if only one RF subcarrier is used per RBS and a linearized optical modulator is employed, since all of the optical carrier and signals from previous RBSs are modulated together in the RBS.

This chapter proposes novel cascaded radio-on-fiber systems in which no intermodulation distortion due to cascaded modulators occurs in the uplink. Also, no beat noise caused by the use of multiple light sources occurs. In order to improve the performance of the proposed cascaded ROC systems, the optimization of the optical modulation index in each RBS is proposed. The carrier-to-noise ratio (CNR) performances of the cascaded ROC/HD system and cascaded ROC/SHD system are theoretically analyzed and compared with that of the conventional cascaded IM/DD system.

In the cascaded IM/DD system, since the intermodulation distortion due to cascaded modulators occurs even if only one radio subcarrier is used per RBS and the optical modulation scheme has an ideal linear characteristic. Therefore, to analyze the fundamental merit of the proposed system, one radio subcarrier per RBS is assumed in this study.

In the downlink, bus-type link, for example, may be employed in the proposed system. However, there is no new configuration particularly for the ROC scheme in the downlink of the proposed system. Also, the downlink tends to have fewer problems than the uplink. Therefore, this chapter deals mainly with the uplink only.

4.2 Principle of Cascaded Radio-to-Optic Direct Conversion Network

Figure 4.2 shows the frequency spectrum of the optical signal at each stage in the RBS. In the proposed cascaded systems, the pilot carrier, $g_p(t)$, and signals from the previous stations: $g_1(t)$, $g_2(t)$,..., $g_{k-1}(t)$, are transmitted to an arbitrary k-th RBS. Then, in order to prevent from the intermodulation distortion, the pilot carrier is divided from the signals ($g_1(t)$, $g_2(t)$,..., $g_{k-1}(t)$) by a frequency splitter. By the use of only the pilot carrier, the ROC converts the RF signal at the k-th RBS to an optical signal. Then, all optical components are combined together again by a frequency combiner. Since only the pilot carrier component is modulated by the RF signal, therefore no intermodulation distortion occurs.

The frequency splitter and the frequency combiner can be realized by using the wavelength demultiplexer and the wavelength multiplexer, both of which are used in WDM systems, respectively. In the proposed cascaded ROC systems, RF subcarriers are considered

to be in millimeter-wave (mm-wave) frequency band, e.g. 60 GHz, therefore the frequency splitter and the frequency combiner (for instance, array waveguide gratings (AWGs)) can split or combine the pilot carrier component and the signal component without substantial problem [61],[62].

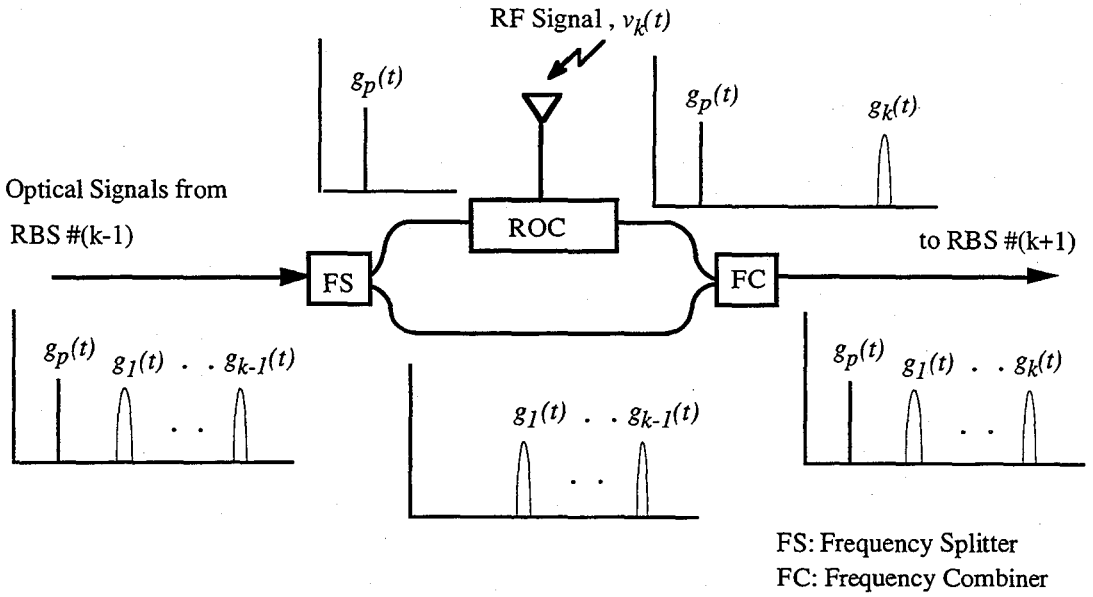

Figure 4.2: Frequency Spectrum of the Optical Signal at Each Stage in the RBS.

4.3 System Configuration

4.3.1 Cascaded ROC/Heterodyne Detection System

Figure 4.3 shows the configuration of the proposed cascaded ROC systems. At the first RBS, neither frequency splitter nor frequency combiner is required because there is still no optical signal component transmitted to this RBS. At the input of the second RBS or any other RBSs after the second RBS, signals from the previous stations and the pilot carrier are transmitted through the polarization controller in order to match the state of polarization of the light with the axis of the ROC. Then, the pilot carrier is divided from the signals by the use of the frequency splitter. After the ROC converts the RF signal received at the RBS to an optical signal, all optical components are combined together again by the frequency combiner. The propagation loss of the optical fiber between two neighboring RBSs and the insertion loss in the RBS can be compensated by an optical amplifier. Finally, all optical components are

transmitted to the next RBS.

At the CS, in the case of HD shown in Fig. 4.3 (a), the received light is detected by a balanced mixing photodetector after matching the state of polarization of the received light with that of the LO light by the polarization controller. The RF signals are regenerated after passing through the BPFs.

4.3.2 Cascaded ROC/Self-Heterodyne Detection System

Figure 4.3 (b) shows the configuration of the cascaded ROC/SHD system. Although the pilot

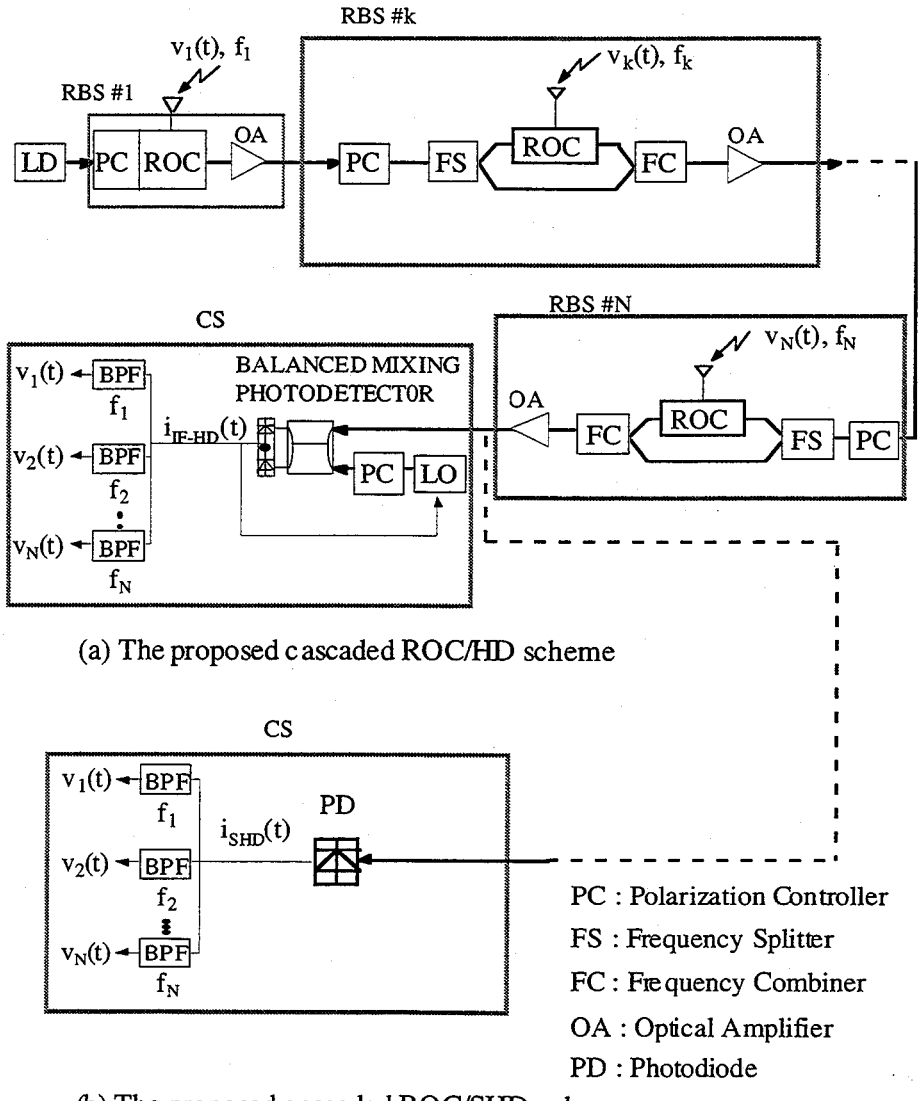

Figure 4.3: Configuration of the Proposed Cascaded ROC Systems.

carrier is used in each RBS in the cascade link, the SHD scheme can be employed if there is enough power of the pilot carrier received at the CS. As described in subsection 3.2.2, in the cascaded ROC/SHD system, the LO, the frequency control, the state of polarization control are not necessary and the receiver structure becomes simple.

4.4 Theoretical Analysis of Received Carrier-to-Noise Ratio

In this study, the received CNR of the cascaded ROC systems are theoretically analyzed assuming 1 subcarrier per RBS.

4.4.1 Cascaded ROC/Heterodyne Detection System

In the case of heterodyne detection, the LO light is

$$g_L(t) = \sqrt{2P_L}\, e^{j\{2\pi f_L t + \phi_L(t)\}} \tag{4.1}$$

where P_L, f_L, and $\phi_L(t)$ are the power, frequency, and phase noise of the LO, respectively. The intermediate frequency (IF) current after the balanced mixing photodetector is

$$i_{IF-HD}(t) = i_{C-HD}(t) + \sum_{k=1}^{N} i_{k-HD}(t) + n_{HD}(t) \tag{4.2}$$

where $i_{C\text{-}HD}(t)$, $i_{k\text{-}HD}(t)$, N, and $n_{HD}(t)$ are the carrier, the signal from the k-th RBS, the number of RBSs connected in the system, and the noise, respectively. The photocurrents of the carrier and the signal from the k-th RBS can be expressed by

$$i_{C-HD} = 2e\alpha\sqrt{P_C P_L}\cdot\cos[2\pi f_{IF} t + \Delta\phi(t)] \tag{4.3}$$

$$i_{k-HD} = 2e\alpha\sqrt{P_{r,k} P_L}\cdot\cos[2\pi(f_{IF} + f_{RF} + k\Delta f)t + \Delta\phi(t) + \theta_k(t)] \tag{4.4}$$

where e, α, P_C, $P_{r,k}$, f_{IF}, f_{RF}, Δf, $\Delta\phi(t)$, and $\theta_k(t)$ are the electron charge, the electro-optic constant, the received power of the pilot carrier, the received optical power of the signal from the k-th RBS, the frequency of the IF signal ($f_{IF} = f_O - f_L$), the subcarrier radio frequency, the

frequency interval between two adjacent RF signals , the phase noise of the optical signal ($\Delta\phi(t) = \phi_O(t) - \phi_L(t)$), and the phase of the k-th RF signal, respectively. At the receiver, the loss of the optical signal component modulated by the RF signal in RBS #k is

$$Loss_k = L_f + N \cdot L_S + k \cdot L_m + (N-1) \cdot L_d \tag{4.5}$$

$$L_f = (N+1) \cdot L_{f'} \tag{4.6}$$

where L_f , $L_{f'}$, L_S , L_m and L_d are the total fiber propagation loss of the link, the fiber propagation loss between two adjacent RBSs, the insertion loss of the polarization controller, the modulator, and the frequency splitter together with the frequency combiner, respectively. The received optical power of the pilot carrier, P_C, and the received optical power of the signal from the k-th RBS, $P_{r,k}$, can be expressed as

$$P_c = P_t L_f \cdot \left[\prod_{k=1}^{N} \cos(\pi OMI_k)\right]^2 \tag{4.7}$$

$$P_{r,k} = P_t Loss_k \cdot \left[\sin(\pi OMI_k) \cdot \left\{\prod_{j=1}^{k-1} \cos(\pi OMI_j)\right\}\right]^2 \tag{4.8}$$

where P_t is the transmitting optical power and OMI_k is the optical modulation index (OMI) of the k-th RBS defined by

$$OMI_k = \frac{A_k}{V_\pi} \tag{4.9}$$

where A_k is the amplitude of the k-th RF signal. Hence, the power of the signal from the k-th RBS is

$$P_{HD,k} = 2e^2\alpha^2 P_{r,k} P_L \tag{4.10}$$

Considering the relative intensity noise (RIN), the signal and the LO shot noises, and the receiver thermal noise, the total noise power can be given by

$$\sigma^2_{HD,total} = \left\{ RIN e^2 \alpha^2 P_r P_L + 2e^2 \alpha P_r + 2e^2 \alpha P_L + \frac{8k_B T}{R_L} \right\} B \tag{4.11}$$

where P_r, B_o, k_B, T, R_L and B are the total received optical power, the bandwidth of an optical filter, the Boltzmann constant, the noise temperature, the load resistance, and the RF signal bandwidth, respectively. The four terms on the right-hand side of Eq. (4.11) are the RIN, the signal shot noise, the LO shot noise, and the receiver thermal noise, respectively. The total received optical power, P_r, can be written as

$$P_r = P_c + \sum_{k=1}^{N} P_{r,k} \tag{4.12}$$

Therefore, the received CNR of the RF signal from the k-th RBS is

$$CNR_{HD,k} = \frac{P_{HD,k}}{\sigma^2_{HD,total}} \tag{4.13}$$

In the case of using optical amplifiers in RBSs to compensate the loss in the link, the loss between each amplifier can be expressed as

$$L_{sub} = L_f L_S L_m L_d \tag{4.14}$$

The gain of the optical amplifier in each RBS is assumed to be identical to all losses between itself and the previous optical amplifier, thus

$$G_1 = \frac{1}{L_S L_m} \quad \text{for the amplifier in the first RBS} \tag{4.15}$$

$$G = \frac{1}{L_{sub}} \quad \text{for the amplifiers in other RBSs} \tag{4.16}$$

In cascade-link systems, the ASE noises accumulate and are amplified at the following amplifiers. At the receiver input, the accumulated ASE noises can be considered as white noise throughout the total subcarrier signal band, therefore, the ASE noise has the same

power density in each RF signal band. Assuming that frequency splitters and frequency combiners can split and combine frequency spectrum perfectly, the power spectral density of the amplified spontaneous emission (ASE) received at the receiver is [63],[64]

$$N_{ASE} = \frac{n_{sp}(G_1 - 1)h\nu + (p-1)n_{sp}(G-1)h\nu}{L_f} \tag{4.17}$$

where n_{sp}, h , ν, and p are the ASE coefficient, Planck's constant, the optical frequency, and the number of optical amplifiers, respectively. The IF current after the balanced mixing photodetector can be expressed by Eq. (4.2). The received power of the pilot carrier, $P_{C(OA)}$, and the received optical power of the signal from the k-th RBS, $P_{r,k(OA)}$, can be expressed as

$$P_{c(OA)} = P_t L_f \cdot \left[\prod_{k=1}^{N} \cos(\pi OMI_k)\right]^2 \tag{4.18}$$

$$P_{r,k(OA)} = P_t Loss_k \cdot \left[\sin(\pi OMI_k) \cdot \left\{\prod_{j=1}^{k-1} \cos(\pi OMI_j)\right\}\right]^2 \tag{4.19}$$

The power of the signal from the k-th RBS is given by Eq. (4.10). Considering the RIN, ASE noise, the signal and the LO shot noises, and the receiver thermal noise, the total noise power can be given by

$$\begin{aligned}\sigma^2_{HD,total(OA)} = \{&RIN e^2\alpha^2 P_r P_L + 2e^2\alpha P_r + 2e^2\alpha P_L \\ &+ 2e^2\alpha N_{ASE} B_o + \frac{8k_B T}{R_L} + 4e^2\alpha^2 P_L N_{ASE} \\ &+ 4e^2\alpha^2 P_r N_{ASE} + 4e^2\alpha^2 N^2_{ASE} B_o\} B\end{aligned} \tag{4.20}$$

where B_o is the ASE bandwidth limited by an optical filter. The eight terms on the right-hand side of Eq. (4.20) are the RIN, the signal shot noise, the LO shot noise, the ASE shot noise, the receiver thermal noise, the LO-spontaneous emission beat noise, the signal-spontaneous emission beat noise, and the spontaneous-spontaneous emission beat noise, respectively. The total received optical power, P_r , is given by Eq. (4.12). Therefore the received CNR of the RF signal from the k-th RBS is

$$CNR_{HD,k(OA)} = \frac{P_{HD,k(OA)}}{\sigma^2_{HD,total(OA)}} \tag{4.21}$$

4.4.2 Cascaded ROC/Self-Heterodyne Detection System

In the case of the cascaded ROC/SHD system, the output current after the photodiode is

$$i_{SHD}(t) = \sum_{k=1}^{N} i_{k-SHD}(t) + n_{SHD}(t) \tag{4.22}$$

where $i_{k\text{-}SHD}(t)$ and $n_{SHD}(t)$ are the signal from the k-th RBS and the noise, respectively. The signal from the k-th RBS, $i_{k\text{-}SHD}(t)$, can be expressed by

$$i_{k-SHD} = 2e\alpha\sqrt{P_{r,k}P_C}\cdot\cos[2\pi(f_{RF}+k\Delta f)t+\theta_k(t)] \tag{4.23}$$

Hence, the power of the signal from the k-th RBS is

$$P_{SHD,k} = 2e^2\alpha^2 P_{r,k}\,P_c \tag{4.24}$$

where P_c and $P_{r,k}$ are given by Eq. (4.7) and (4.8), respectively. The total noise power can be written as

$$\sigma^2_{SHD,total} = \left\{RIN\,e^2\alpha^2P_r^2 + 2e^2\alpha P_r + \frac{4k_BT}{R_L}\right\}B \tag{4.25}$$

where P_r is given by Eq. (4.12). Therefore, the received CNR of the RF signal from the k-th RBS is

$$CNR_{SHD,k} = \frac{P_{SHD,k}}{\sigma^2_{SHD,total}} \tag{4.26}$$

In the case of using optical amplifiers in RBSs to compensate the loss in the link, the power of the signal from the k-th RBS is given by

$$P_{SHD,k(OA)} = 2e^2\alpha^2 P_{r,k(OA)} P_{c(OA)} \tag{4.27}$$

where $P_{C(OA)}$ and $P_{r,k(OA)}$ are given by Eq. (4.18) and (4.19), respectively. The total noise power can be written as

$$\begin{aligned}\sigma^2_{SHD,total(OA)} = \{&RIN\, e^2\alpha^2 P_r^2 + 2e^2\alpha P_r + 2e^2\alpha N_{ASE} B_o \\ &+ \frac{4k_B T}{R_L} + 4e^2\alpha^2 P_r N_{ASE} + 4e^2\alpha^2 N_{ASE}^2 B_o\} B\end{aligned} \tag{4.28}$$

Consequently, the received CNR of the RF signal from the k-th RBS is

$$CNR_{SHD,k(OA)} = \frac{P_{SHD,k(OA)}}{\sigma^2_{SHD,total(OA)}} \tag{4.29}$$

4.5 Numerical Results and Discussions

Table 1 shows the parameters used in calculations. In the calculation, the distance between two adjacent RBSs is assumed to be 100 m, therefore the fiber propagation loss, L_f., between two adjacent RBSs is assumed to be 0.02 dB. Linearized external intensity modulators are assumed to be employed in the conventional cascaded IM/DD system.

Table 2 Parameters used in calculations

Local Light Power: P_L	10 dBm
Relative Intensity Noise: RIN	-152 dB/Hz
Photodiode: r	0.8 A/W
Load Resistance: R_L	50 Ω
Noise Temperature: T	300 K
Spontaneous Emission Factor: n_{sp}	1.0
ASE Bandwidth: B_o	1 THz

Figure 4.4 shows the relationship between the received CNR for ROC systems or the received CDNR for the IM/DD system and the order of RBS, k, in the case of using identical OMI in every RBS and using the optical amplifier in each RBS. The number of the RBSs connected in the system, N, is assumed to be 10. In the proposed ROC systems, when all of the OMIs are set to be equal to each other, the CNR of the signal from the RBS nearest to a CS is smaller than those from other RBSs. This is because the optical carrier left to this RBS has the smallest power due to its use for modulation in previous RBSs. In the case of setting an equal value to every OMI, therefore, we set the OMI to be the one which maximizes the CNR of the RBS nearest to the CS. If the OMI is too small, although the optical carrier left to the nearest RBS is still large, but the CNR of this RBS is small due to the small value of OMI. If the OMI is too large, the optical carrier left to this RBS is small, thus the CNR of this RBS becomes small. The OMI of 0.036 in the ROC/HD system and 0.015 in the ROC/SHD system are obtained by using the method above. In the rest of this chapter, we will refer to the CNR of the RBS nearest to the CS when we discuss cascaded ROC systems in the case of using identical OMI in every RBS.

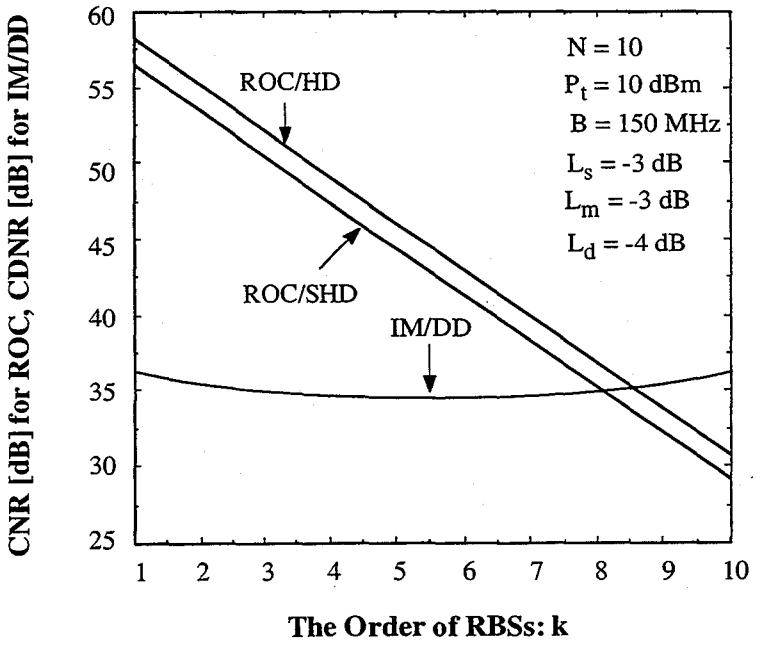

Figure 4.4: Relationship between the Received CNR and the Order of RBSs in the Case of Using Identical OMI in Every RBS.

In the cascaded IM/DD system, the CDNR of the signal from the middle RBS in the link is the smallest because the cascaded connection generates the maximum value of intermodulation distortion in the middle subcarrier frequency band (see Appendix B). In this calculation, the OMI of 0.041 is the one which maximizes the CDNR of the middle RBS. If the OMI is higher than this value, the CDNR is degraded by the intermodulation distortion.

It can be seen that the received CNR of the ROC/SHD system is approximately 2 dB less than that of the ROC/HD system. This is due to the fact that, in the ROC/SHD system, the received power of the pilot carrier which is utilized as the local oscillator, is decreased but not much because the OMI of each RBS is very small.

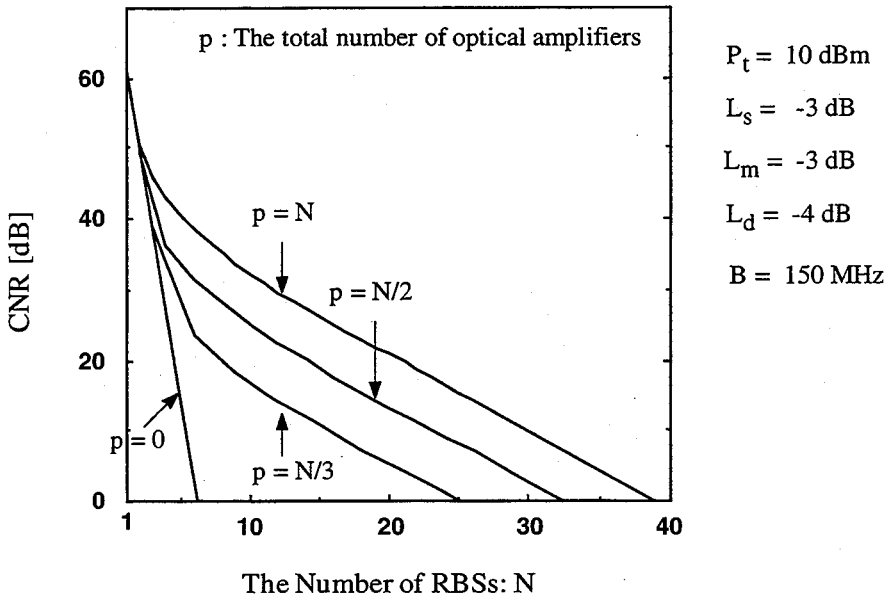

Figure 4.5: Relationship between the Received CNR and the Number of Connected RBSs in the Case of the Cascaded ROC/HD System.

Figure 4.5 shows the relationship between the received CNR and the number of connect RBSs with the number of optical amplifiers, *p*, as a parameter, in the case of using identical OMI in every RBS. The graphs of the systems which use the optical amplifier in every two RBSs and three RBSs are also shown. Since the insertion losses of the polarization controllers, frequency splitters, and frequency combiners are included in the cascaded ROC systems, the CNR performance in the case of not using optical amplifiers is poor. These losses can be compensated by employing optical amplifiers. As the total number of optical amplifiers

increases, the received CNR increases, although the gain of optical amplifiers in each case is adjusted so that the total gain in the link in each case is the same as each other. This is because as the total number of optical amplifiers decreases, the total amplified spontaneous emission noise in the link increases, therefore the received CNR decreases.

4.6 Optimization of Optical Modulation Indices

If we set the OMI of each of the RBSs so that the OMI of the RBS farther from the CS is smaller than those of the RBSs nearer to the CS, the received CNR of the signal from the RBS far from the CS will decrease, and that of the signal from the RBS near to the CS will increase. Therefore we can optimize the received CNR performance in the sense that we set each OMI differently so that the received CNR of the RBS nearest to the CS increase and equals that of the RBS farthest from the CS. Hence, to determine each OMI, we get

$$CNR_k = CNR_{k+1} \quad (k = 1,2,...,N-1) \tag{4.30}$$

From the relation above, in the case of both ROC/HD and ROC/SHD systems, it can be expressed as

$$(\sin \pi OMI_k)^2 = L_m (\sin \pi OMI_{k+1})^2 (\cos \pi OMI_k)^2 \tag{4.31}$$

Thus, the optimum OMI of the k-th RBS is

$$OMI_k = \frac{1}{\pi} \arctan\left(\sqrt{L_m} \cdot \sin \pi OMI_{k+1}\right) \tag{4.32}$$

To determine the optimum OMIs, we start from setting the OMI of the N-th RBS which is nearest to the CS, and then use Eq. (4.32) to determine the OMIs of the (N-1)-th, (N-2)-th,..., and the 1st RBS, respectively. In the ROC/HD system, the OMI of the N-th RBS is firstly set to 0.5, i.e. using up the whole optical pilot carrier to achieve the maximum received CNR. In the ROC/SHD system, however, the received CNR also depends on the received power of the optical pilot carrier as shown in Eq. (4.24). Therefore, the OMI of the N-th RBS should be set to a certain value to remain the appropriate power in the optical pilot carrier for self-heterodyne detection. In this calculation, the signal-ASE beat noise is dominant, and the OMI

of the N-th RBS in the ROC/SHD system which maximizes the received CNR is found to be 0.11. Figure 4.6 shows the relationship between the optimized OMI and the order of RBS in the case of ROC modulator insertion loss of 3 dB. It can be seen that the farther the RBS is located from the CS, the smaller the OMI of that RBS becomes, so that there is still enough power of the optical carrier left to the RBS nearer to the CS. It can also be seen that if a new RBS is added to the RBS farthest from the CS, we just have to set the optimum OMI of the new RBS without any change in other OMIs.

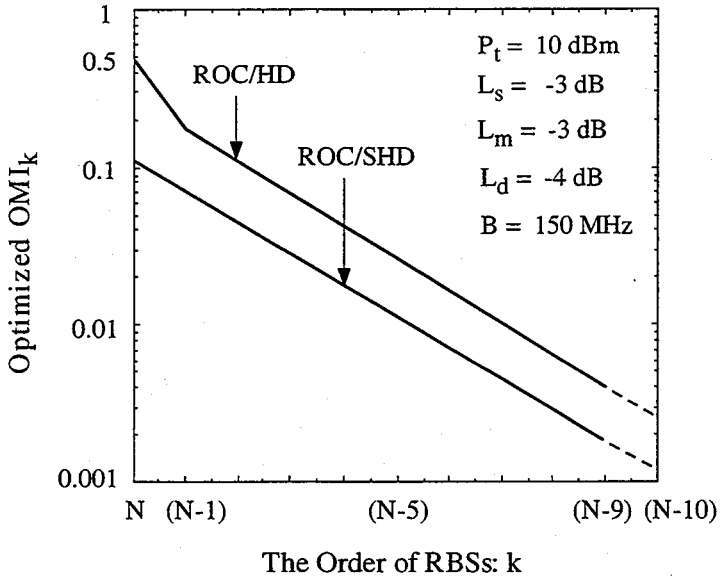

Figure 4.6: Relationship between the Optimized OMI and the Order of RBSs.

4.7 Evaluation of Received CNR Performance Improvement

Figure 4.7 shows the relationship between the received CNR for ROC systems or the received CDNR for IM/DD systems and the number of RBSs with the RF signal bandwidth as a parameter, in the case of using the optical amplifier in each RBS. Here, the OMIs of the ROC systems are optimized using the proposed OMI optimization method. As a result, the received CNR of the RBS nearest to the CS in the case of using optimized OMIs shows a significant improvement over that in the case of using identical OMIs. The ROC systems using optimized OMIs also provide improvement in the received CNR over the CDNR of the IM/DD system, this is because the intermodulation distortion due to cascaded connection

occurs in the IM/DD system when the number of RBSs is more than two, deteriorating the received CDNR severely. In the case of RF signal bandwidth, B, of 150 MHz and $N = 20$, the ROC/HD and the ROC/SHD systems provide approximately 16 dB and 14 dB improvement over the IM/DD system, respectively. The difference between the received CNR of the ROC/HD system and the ROC/SHD system is approximately 2 dB which is the larger than that in the case of using identical OMI for every RBS. This is due to the fact that the entire pilot carrier cannot be used up to achieve the maximum received CNR performance for the ROC/HD system in the case of using identical OMI. In the case of $B = 50$ MHz and $N = 20$, the ROC/HD and the ROC/SHD systems provide approximately 18 dB and 16 dB improvement over the IM/DD system, respectively. The improvement is better than that in the case of $B =$ 150 MHz. This is because, as B decreases, the received CDNRs of the IM/DD system do not become as much higher as those in the ROC systems, due to the intermodulation distortion.

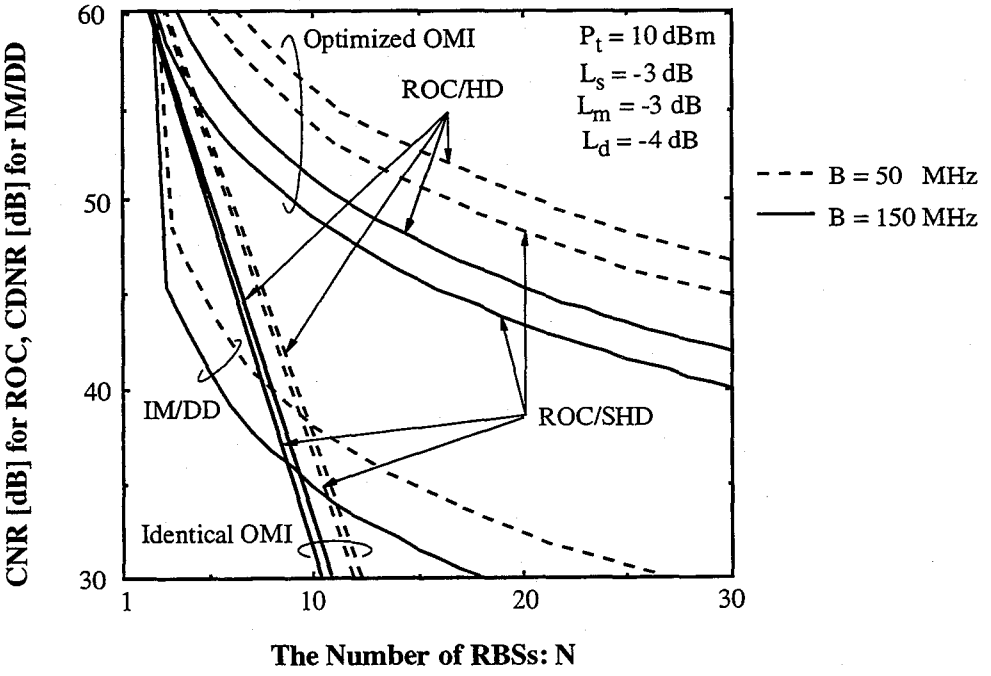

Figure 4.7: Relationship between the Received CNR and the Number of Connected RBSs.

In the case of adding a new RBS to the RBS farthest from the CS, the optimized OMI for the new RBS has already been derived by the proposed method, and no OMI re-optimization of the rest of the RBSs is required. On the other hand, in the case of adding a new RBS between any two RBSs, how to determine the OMI for the new RBS is to use the average

value of the OMIs of its neighbor RBSs. This value can be considered as a sub-optimum OMI. Figure 4.8 shows the relationship between the received CNR degradation and the order of RBS in the case of adding new RBSs in the ROC/HD system, and using the sub-optimum OMIs instead of re-optimization. One, two or four RBSs are added in a 10-RBS system behind the RBS number shown in the horizontal axis. Here, the CNR degradation denotes the degradation from the CNR obtained in the case of re-optimizing the OMIs. It can be seen from this figure that the CNR degradation occurs when sub-optimum values of OMIs are used. In the ROC/SHD system, the CNR degradation occurs in a very similar pattern as that in the ROC/HD system. We can compensate this degradation by two methods. One method is to prepare a margin in the transmitting optical power level. That is, the transmitting optical power is set below its maximum power in the beginning, and will be increased when new RBSs are added. The other one is re-optimization of all of the OMIs. The former method may be applied first, and when the transmitting optical power reaches its maximum available level, the re-optimization is performed.

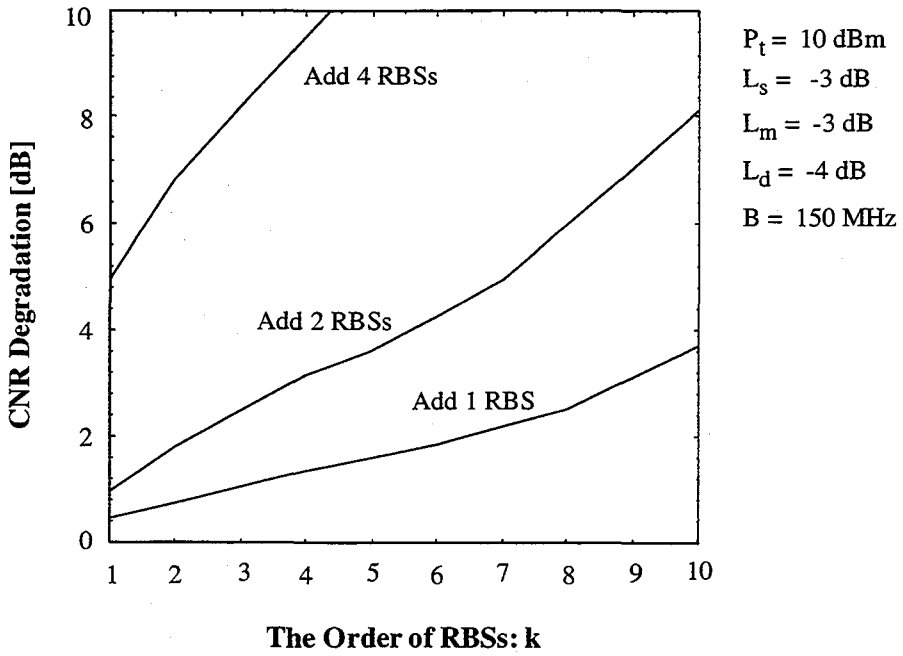

Figure 4.8: Relationship between the Received CNR Degradation and the Order of RBSs in the Case of Adding New RBSs in ROC/HD System and Using the Sub-optimum OMIs Instead of Re-optimization (One, two, or four RBSs are added in a 10-RBS system behind the RBS number shown in the horizontal axis).

In addition, the selection of the compensation method depends on the location of the added RBS. As shown in Fig. 4.8, without re-optimization, fewer RBSs can be added to the RBSs located near the CS because the OMIs of these RBSs are relatively high, therefore assigning an average value of OMI of two neighbor RBSs to the new OMI without re-optimization deteriorates the CNR more severely in this region. Re-optimization should be more appropriate in this case.

Figure 4.9 shows the relationship between the maximum connected number of RBSs and the insertion loss of the optical modulator in the case of using optical amplifier in each RBS. Since the IM/DD system has only the loss of the modulator, therefore, to compare the proposed system with the IM/DD system fairly, only the loss of the modulator is expressed on the horizontal axis. In this calculation, it is assumed that the required CNR (CDNR for IM/DD systems) is 32 dB including the margin of 20 dB. This required CNR corresponds with the value to obtain the required bit error probability of 10^{-6} for a quarternary phase shift keying

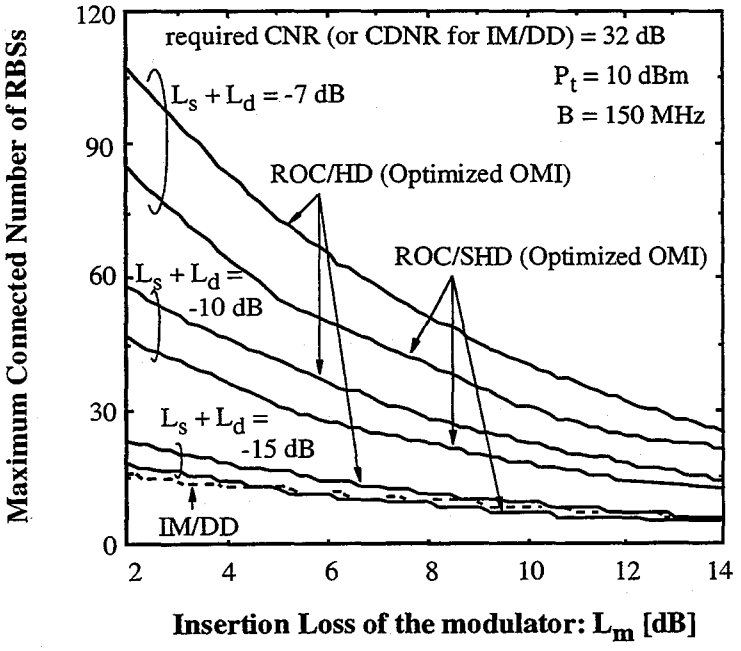

Figure 4.9: Relationship between the Maximum Connected Number of RBSs and the Insertion Loss of the Modulator.

(QPSK) signal. We can see that, the ROC/HD and ROC/SHD systems using optimized OMIs can accommodate much more RBSs than the IM/DD system even in the relatively high insertion loss of the modulator region. The ROC/SHD system, for example, can accommodate at least 2 times as many RBSs as the IM/DD system in the case of total loss of the polarization controller, frequency splitter and frequency conbiner of 10 dB. The performance of ROC systems degrades to approximately same level as IM/DD systems when total loss of the polarization controller, frequency splitter and frequency conbiner is 15 dB.

Regarding the nonlinearity of each modulator, although the effects are not exactly the same in the proposed systems and the IM/DD system, it is a common factor in both systems. Thus, in order to analyze the fundamental merit of the proposed system, it is ignored in this study. Therefore, this chapter does not include the nonlinearity in each modulator, RBS's receiver dynamic range, and the spurious characteristics.

When the number of radio subcarriers is more than 1, the intermodulation distortion is induced by the nonlinearity of the ROC modulator. The investigation of this distortion has been performed in Chapter 3. In this case, despite of the CDNR degradation, the merit of the proposed cascade system still remains, because the merit is to eliminate the carrier-to-distortion-plus-noise-power ratio (CDNR) degradation due to the intermodulation distortion induced by the cascaded modulators.

4.8 Concluding Remarks

This chapter proposed a novel cascade-type inter-cell connection link for radio-on-fiber systems. The received CNR performances of the proposed cascaded systems employing the ROC/HD and ROC/SHD schemes were theoretically analyzed. The optimization of the optical modulation index (OMI) in each RBS was also presented. The following results were found:

1. In the case of using identical OMI in every RBS, the received CNR of the RF signal from the RBS nearest to the CS is the smallest.

2. Degraded received CNR performance in the cascaded ROC systems due to the insertion loss of the polarization controllers, frequency splitters, and frequency combiners, can be substantially improved by employing optical amplifiers.

3. The received CNR of the RF signal from the RBS nearest to the CS can be improved greatly by the proposed OMI optimization method.

By using the proposed optical modulation index optimization method and employing the optical amplifier in each RBS, the following results were obtained:

4. In the case of the RF signal bandwidth of 150 MHz and the number of RBSs of 20, the ROC/HD and the ROC/SHD systems were shown to provide approximately 16 dB and 14 dB improvement of the received CNR over the received CDNR of the IM/DD system, respectively. This is because, in the IM/DD system, the intermodulation distortion due to cascaded connection of optical modulators occurs and deteriorates the received CDNR severely. On the other hand, no such intermodulation distortion occurs in the proposed cascaded ROC systems.

5. In the case of adding a new RBS to the RBS farthest from the CS, we only have to set the optimum OMI, which can be determined in advance by the proposed OMI optimization method, to the new RBS. No change in other OMIs is required.

6. The ROC/HD and ROC/SHD systems using optimum OMIs can accommodate much

more RBSs than the IM/DD system even in the case of relatively high modulator insertion loss. The ROC/SHD system, for example, can accommodate at least 2 times as many RBSs as the IM/DD system in the case of total insertion loss of the polarization controller, frequency splitter and frequency combiner of 10 dB.

Chapter 5

Conclusions

This thesis proposed subcarrier multiplexing radio-to-optic direct conversion systems and novel cascaded radio-to-optic direct conversion systems for radio-on-fiber networks. The received CDNR performance of the ROC/HD system and ROC/SHD system for SCM radio-on-fiber systems were theoretically analyzed taking into account their intermodulation distortion caused by nonlinear modulation characteristics. The received CDNR performance and the SFDR performance of both of the ROC systems were discussed and compared with those of the conventional DMZ/HD, CPM/HD and IM/DD systems. The novel cascaded ROC systems were proposed in order to eliminate the intermodulation distortion, which arises in the systems that employ the conventional cascade-type link. The received CNR performances of the proposed cascaded ROC/HD system and cascaded ROC/SHD system were theoretically analyzed, discussed and compared with that of the conventional cascaded IM/DD system. The optimization of the optical modulation index in each of the RBSs was presented in order to improve the received CNR performance the proposed systems.

Through the analysis in Chapter 3, which dealt with the SCM ROC systems, the following results were obtained:

- The SCM ROC/HD system can improve the received CDNR performance over the DMZ/HD and CPM/HD systems by approximately 5 dB and 2.5 dB, respectively, for every number of channels. This is due to the fact that the ROC scheme can allocate the optical power solely to the first order component, while in both DMZ and CPM schemes, some optical power is used in the third order and higher order harmonics. In the case of multi-octave RF SCM signal, the ROC, DMZ and CPM systems are not affected by the second order intermodulation distortion, and can remarkably improve the CDNR over the conventional AM/HD and IM/DD systems.

- The SCM ROC/SHD system can improve the received CDNR performance over the conventional IM/DD system by approximately 5 dB for the received optical power of less than -10 dBm. This is because the received RF power of the ROC/SHD system is larger than that of the IM/DD system, and in this region, the power of the intermodulation distortion which depends on the received optical power is small, thus, the effect of the intermodulation distortion which is larger in the ROC/SHD system than in the IM/DD system diminishes.

- The SFDRs of the SCM ROC/HD system are 42.1 dB and 56.8 dB in the case of the received optical power of -5 dBm and the number of channels of 20, for the RF signal bandwidth of 150 MHz and 1 MHz, respectively. These SFDRs are approximately 2 dB and 4 dB improved over those of the CPM/HD and DMZ/HD systems, respectively.

- The SFDRs of the SCM ROC/SHD system are 35.3 dB and 50.1 dB in the case of the received optical power of -5 dBm and the number of channels of 20, for the RF signal bandwidth of 150 MHz and 1 MHz, respectively. The SFDR of the ROC/SHD system is approximately the same as that of the IM/DD system whose 3rd order laser diode nonlinear coefficient is 0.01. This is because, although the received RF power of the ROC/SHD system is larger than that of the IM/DD system, but the intermodulation distortion power of the ROC/SHD system is larger than that of IM/DD system due to the existence of the pilot IM2.

Through the analysis in Chapter 4, which proposed the novel cascaded ROC systems, the following results were obtained:

- The proposed cascaded ROC systems can eliminate the intermodulation distortion due to conventional cascade connection. However, the received CNR of the RF signal from the RBS nearest to the CS is the smallest in the case of using identical OMI in every RBS. Degraded received CNR performance in the cascaded ROC systems due to the insertion loss of the polarization controllers, frequency splitters, and frequency combiners, can be substantially improved by employing optical amplifiers. In addition, the received CNR of the RF signal from the RBS nearest to the CS can be improved remarkably by the proposed optical modulation index (OMI) optimization method.

By using the proposed OMI optimization method and employing the optical amplifier in each RBS, the following results were obtained:

- The cascaded ROC/HD and cascaded ROC/SHD systems can provide about 16 dB and 14 dB improvement of the received CNR over the received CDNR of the cascaded IM/DD system, respectively, in the case of the RF signal bandwidth of 150 MHz and the number of RBSs of 20.

- In the case of adding a new RBS to the RBS farthest from the CS, we only have to set the optimum OMI, which can be determined in advance by the proposed OMI optimization method, to the new RBS. No OMI re-optimization of the rest of the RBSs is required.

- The cascaded ROC/HD and cascaded ROC/SHD systems using optimum OMIs can accommodate much more RBSs than the cascaded IM/DD system even in the case of high modulator insertion loss. The cascaded ROC/SHD system, for instance, can accommodate at least two times as many RBSs as the cascaded IM/DD system in the case of the total loss of the polarization controller, frequency splitter and frequency combiner of 10 dB.

The radio-on-fiber networks will become more and more important key technology for the infrastructure of future personal mobile communication systems in which the flexibility and universality to various kinds of multimedia wireless services are significant. The ROC systems treated in this thesis will become one of the candidates for the systems applied to such flexible radio access networks. The author wishes that the results of this research contribute toward the technological development of future radio-on-fiber networks.

Appendix

Appendix A: Received CDNR of the SCM IM/DD System

In the cascaded IM/DD system employing direct modulation of the laser diode, with the intensity modulation index, m, and taking into account the relative intensity noise, shot noise, receiver thermal noise, and intermodulation distortion, the received CDNR can be expressed as [25]

$$CDNR = \frac{\frac{1}{2} r^2 P_R{}^2 m^2}{\sigma_{IM3}{}^2 + (RIN\, r^2 P_R{}^2 + 2erP_S + \frac{4kT}{R_L})B} \tag{A.1}$$

where σ^2_{IM3} is the power of IM3, given by

$$\sigma_{IM3}{}^2 = \frac{1}{2} r^2 P_R{}^2 \left\{ \left[(\frac{3}{4} c_3 m^3) \cdot D_2(N,k) \right] + \left[(\frac{3}{2} c_3 m^3) \cdot D_3(N,k) \right] \right\}^2 \tag{A.2}$$

where $D_2(N,k)$ and $D_3(N,k)$ are the number of two-tone IM3 and of three-tone IM3, respectively. c_i (i=2,3,...) are the photodiode nonlinear coefficients. $D_2(N,k)$ and $D_3(N,k)$ are written respectively as

$$D_2(N,k) = \frac{1}{2} \left[N - 2 - \frac{1}{2} \left\{ 1 - (-1)^N \right\} (-1)^k \right] \tag{A.3}$$

$$D_3(N,k) = \frac{k}{2}(N-k+1) + \frac{1}{4} \left\{ (N-3)^2 - 5 \right\} - \frac{1}{8} \left\{ 1 - (-1)^N \right\} (-1)^{N+k} \tag{A.4}$$

Appendix B: Received CDNR of the cascaded IM/DD System

Figure B-1 shows the configuration of the conventional cascaded IM/DD system. The loss between two adjacent amplifiers is given by

$$L_{sub-IM} = L_f L_m \tag{B.1}$$

The gain of each optical amplifier is assumed to be identical to the loss between two adjacent optical amplifiers, thus

$$G_{IM} = \frac{1}{L_{sub-IM}} \quad \text{for all amplifiers} \tag{B.2}$$

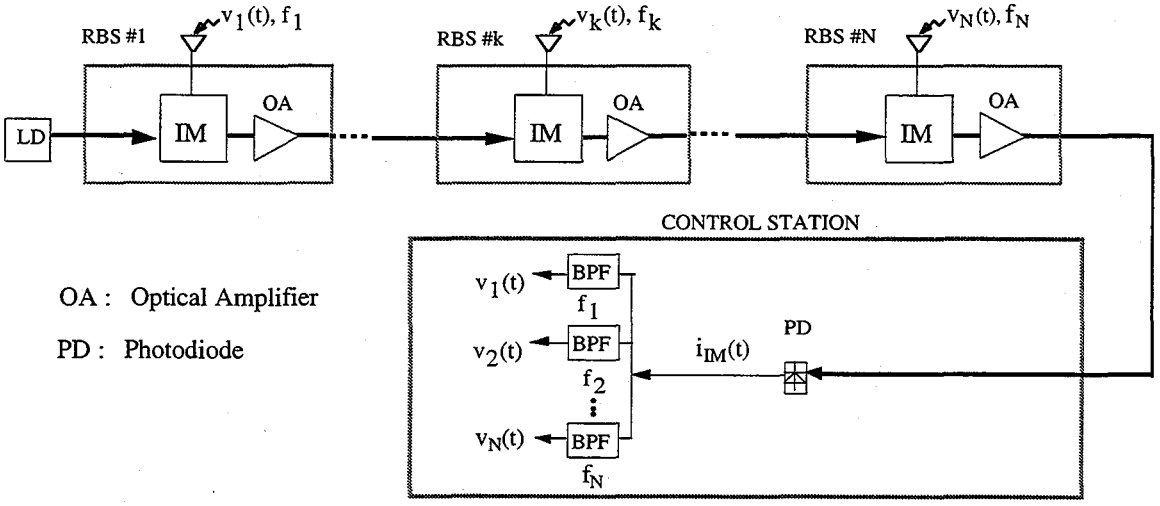

Figure B-1: Configuration of the Conventional Cascaded IM/DD System.

Therefore the power spectral density of the ASE received at the receiver is

$$N_{ASE-IM} = \frac{p\, n_{sp}(G_{IM} - 1)h\nu}{L_f} \tag{B.3}$$

In the case of employing linearized optical intensity modulators, the received optical power at the photodiode is [38]

$$\begin{aligned} P_{IM} &= L_f P_t \prod_{k=1}^{N} (1 + OMI \sin \omega_k t) \\ &= L_f P_t \{1 + OMI \sum_k \sin \omega_k t + \left(\frac{OMI^2}{2}\right) \sum_{k_1 \neq} \sum_{k_2} \cos(\omega_{k_1} \pm \omega_{k_2}) t \\ &+ \left(\frac{OMI^3}{4}\right) \sum_{k_1 \neq} \sum_{k_2 \neq} \sum_{k_3} \sin(\omega_{k_1} \pm \omega_{k_2} \pm \omega_{k_3}) t + \ldots \} \end{aligned} \tag{B.4}$$

The received CDNR of each RF signal is

$$CDNR_{IM} = \frac{\frac{1}{2} e^2 \alpha^2 (P_t L_f)^2 OMI^2}{\sigma^2_{noise} + \sigma^2_{IM3}} \tag{B.5}$$

where σ^2_{noise} is the total noise power and σ^2_{IM3} is the power of the IM3, which can be expressed by

$$\begin{aligned} \sigma^2_{noise} &= \{RIN e^2 \alpha^2 (P_t L_f)^2 + 2e^2 \alpha (P_t L_f) + 2e^2 \alpha N_{ASE-IM} B_o \\ &+ \frac{4k_B T}{R_L} + 4e^2 \alpha^2 (P_t L_f) N_{ASE-IM} + 4e^2 \alpha^2 N^2_{ASE-IM} B_o \} B \end{aligned} \tag{B.6}$$

$$\sigma^2_{IM3} = \frac{1}{2} e^2 \alpha^2 (P_t L_f)^2 \left(\frac{OMI^3 D_3(N,k)}{4}\right)^2 \tag{B.7}$$

, respectively, where k is the order of RBS and $D_3(N,k)$ is the number of three-tone IM3 given by Eq. (A.4).

The received CDNR of the RF signal from each RBS is not equal to each other because the number (and therefore the power) of the IM3 is different in each RF subcarrier channel. Since the number of the IM3 reaches maximum in the middle channel, the received CDNR of the RF signal from the middle RBS is the smallest.

Appendix C: Acronyms

ASE	amplified spontaneous emission
CPM	cascaded phase modulation
CS	control station
DD	direct detection
DMZ	dual Mach-Zehnder
FC	frequency combiner
FS	frequency splitter
HD	heterodyne detection
HWP	have-wave plate
IF	intermediate frequency
IM	intensity modulation
IM2	second order intermodulation distortion
IM3	third order intermodulation distortion
LO	local oscillator
OA	optical amplifier
OMI	optical modulation index
PBS	polarization beam splitter
PCS	personal communication system
QWP	quarter-wave plate
RBS	radio base station
RF	radio frequency
ROC	radio-to-optic direct conversion
SHD	self-heterodyne detection
SSB	single-sideband

Bibliography

[1] S. Komaki, K. Tsukamoto, S. Hara, and N. Morinaga, "Proposal of fiber and radio extension link for future personal communications", *Microwave and Optical Tech. Letters*, vol. 6, no. 1, pp. 50-55, Jan. 1993.

[2] W. I. Way, "Optical fiber-based microcellular systems: An overview," *IEICE Trans. Commun.*, vol. E76-B, no. 9, pp. 1091-1102, Sept. 1993.

[3] H. Ogawa, "Microwave and millimeter-wave fiber optic technologies for subcarrier transmission systems," *IEICE Trans. Commun.*, vol. E76-B, no. 9, pp. 1078-1090, Sept. 1993.

[4] J. Namiki, M. Shibutani, W. Domon, T. Kanai and K. Emura, "Optical feeder basic system design for microcellular mobile radio," *IEICE Trans. Commun.*, vol. E76-B, no. 9, pp. 1069-1077, Sept. 1993.

[5] S. Komaki, and E. Ogawa, "Trends of fiber-optic microcellular radio communication networks," *IEICE Trans. Electron.*, vol. E79-C, no. 1, pp. 98-104, Jan. 1996.

[6] S. Komaki, K. Tsukamoto, M. Okada, and T. Ishida, "Trends of optically fed wireless communication systems," *Optical and Quantum Electronics*, vol. 30, no. 11-12, pp. 1079-1088, Dec. 1998.

[7] T. S. Chu and M. J. Gans, "Fiber optic microcellular radio," in *Proc. 41st IEEE Vehicular Technology Conf.*, pp. 339-344, June 1991.

[8] M. Shibutani *et al.*, "Feasibility studies on an optical fiber feeder system for microcellular mobile communication systems," in *ICC'91 Conf. Rec.*, vol. 3, pp. 1176-1181, June 1991.

[9] H. Mizuguti, T. Okuno, S. Komaki, and N. Morinaga, "Performance analysis of optical fiber link for microcellular mobile communication systems," *IEICE Trans. Electron.*, vol. E76-C, no. 2, pp. 271-278, Feb. 1993.

[10] J. C. Fan, C. L. Lu, and L. G. Kazovsky, "Dynamic range requirements for microcellular personal communication systems using analog fiber-optic links," *IEEE Trans. Microwave*

Theory Tech., vol. 45, no. 8, pp. 1390-1397, Aug. 1997.

[11] C. Cox III, and R. Helkey, "Techniques and performance of intensity-modulation direct-detection analog optical links," *IEEE Trans. Microwave Theory Tech.*, vol. 45, no. 8, pp. 1375-1380, Aug. 1997.

[12] G. H. Smith, D. Novak, and Z. Ahmed, "Overcoming chromatic-dispersion effects in fiber-wireless systems incorporating external modulators," *IEEE Trans. on Microwave Theory and Techniques*, vol. 45, no. 8, pp. 1410-1415, Aug. 1997.

[13] M. Uehira, M. Nakura, H. Sato, and A. Hashimoto, "ATM wireless access for mobile multimedia: Concept and Architecture," *IEEE Personal Communications*, pp. 39-48, Oct. 1996.

[14] K. Ogawa, A. Hashimoto, and K. Kohiyama, "Advanced wireless access system," *Kluwer Wireless Personal Communications*, vol. 4, no. 3, pp. 325-338, May 1997.

[15] K. Pahlavan, A. Zahedi, P. Krishnamurthy, "Wideband local access: Wireless LAN and Wireless ATM," *IEEE Communications Magazine*, pp. 34-40, Nov. 1997.

[16] MMAC homepage: http://www.arib.or.jp/mmac/e/index.htm

[17] D. Raychaudhuri, L. J. French, R. J. Siracusa, S. K. Biswas, R. Yuan, P. Narasimhan, C. A. Johnston, "WATMnet: a prototype wireless ATM system for multimedia personal communication," *IEEE J-SAC*, vol. 15, no. 1, pp. 83-95, Jan. 1997.

[18] Magic Wand homepage: http://www.tik.ee.ethz.ch/~wand/homepage.html

[19] D. Novak, Z. Ahmed, and R. B. Waterhouse, "Signal generation using pulsed semiconductor lasers for application in millimeter-wave wireless links," *IEEE Trans. on Microwave Theory and Techniques*, vol. 43, no. 9, pp. 2257-2262, Sept. 1995.

[20] R. Hofstetter, H. Schmuck, and R. Heidemann, "Dispersion effects in optical millimeter-wave systems using self-heterodyne method for transport and generation," *IEEE Trans. on Microwave Theory and Techniques*, vol. 43, no. 9, pp. 2263-2269, Sept. 1995.

[21] Y. Ishii, K. Tsukamoto, S. Komaki, and N.Morinaga, "Coherent fiber-optic microcellular radio communication system using a novel RF-to-optic conversion scheme," *IEEE Trans. Microwave Theory and Techniques.*, vol.43, no. 9, pp. 2241-2248, Sept. 1995.

[22] C. F. Buhrer, D. Baird, and E. M. Conwell, "Optical frequency shifting by electro-optic

effect," *Applied Physics Letters*, vol. 1, no. 2, pp. 46-49, Oct. 1962.

[23] J. Park, W. V. Sorin, and K. Y. lau, "Elimination of the fiber chromatic dispersion penalty on 1550nm millimetre-wave optical transmission," *Electron. Lett.*, vol. 33, no. 6, pp. 512-513, Mar. 1997.

[24] T. E. Darcie, "Subcarrier multiplexing for lightwave networks and video distribution systems," *IEEE J. on Selected Area in Commun.*, vol. 8, no. 7, pp. 1240-1248, Sept. 1990.

[25] H. Harada., H. J. Lee, S. Komaki., and N Morinaga, "Performance analysis of fiber-optic millimeter-wave band radio subscriber loop," *IEICE Trans. Commun.*, vol. E76-B, no. 9, pp. 1128-1135, Sept. 1993.

[26] A. P. Foord, P. A. Davies, and P. A. Greenhalgh, "Optical demultiplexing for subcarrier multiplexed systems," *IEEE Trans. on Microwave Theory and Techniques*, vol. 43, no. 9, pp. 2324-2329, Sept. 1995.

[27] K. Emura, "Enabling technologies for SCM based optically fed wireless communication systems," *Optical and Quantum Electronics*, vol. 30, no. 11-12, pp. 1089-1101, Dec. 1998.

[28] P. Suwonpanich, Y. Suda, K. Tsukamoto, and S. Komaki, "Theoretical CDNR analysis on radio-to-optic direct conversion SCM coherent radio-over-fibre system," *Optical and Quantum Electronics*, vol. 30, no. 11-12, pp. 1103-1117, Dec. 1998.

[29] P. Suwonpanich, K. Tsukamoto, and S. Komaki, "Theoretical analysis of spurious-free dynamic range on radio-on-fiber systems using radio-to-optic direct conversion scheme," (in Japanese), *Technical Report of IEICE*, MWP2000-1, pp. 1-8, Oct. 2000.

[30] M. Izutsu, S. Shikama, and T. Sueta, "Integrated optical SSB modulator/frequency shifter," *IEEE J. Quantum Electro.*, vol. QE-17, no. 11, pp. 41-44, Dec. 1996.

[31] C. F. Buhrer, V. J. Fowler, and L. R. Bloom, "Single-sideband suppressed-carrier modulation of coherent light beams," in *Proceeding of the IRE*, vol. 50, no. 8, pp. 1827-1828, Aug. 1962.

[32] T. Yamasaki, H. Masamitsu, and H. Nishihara, "In-line optical waveguide frequency shifter consisting of TE/TM polarization interferometers," (in Japanese), *Tech. Rep. of IEICE.*, CS87-105, Oct 1987.

[33] M. Haruna, T. Yamasaki, H. Hirata, H. Toda, H. Nishihara, "Optical waveguide

wideband frequency shifter in z-propagating $LiNbO_3$ for a laser doppler velocimeter," in *Proc. of 7th Optical Fibre Sensors Conference (OFS7)*, Sydney, Australia, pp. 113-116, Dec. 1990.

[34] Y. Matsunaka and M. Shibutani, "A short-span optical feeder for wireless personal communication systems using multimode fibers," *IEICE Trans. Electron.*, vol.E79-C, no.1, pp.118-123, Jan. 1996.

[35] G. H. Smith, D. Novak, and C. Lim, "A millimeter-wave full-duplex fiber-radio star-tree architecture incorporating WDM and SCM," *IEEE Photon. Technol. Lett.*, vol.10, no.11, pp. 1650-1652, Nov. 1998.

[36] S. Kajiya, K. Tsukamoto, and S. Komaki, "Proposal of fiber-optic radio highway networks using CDMA method," *IEICE Tran. Electron.*, vol.E79-C, no.1, Jan. 1996.

[37] Y. Shoji, K. Tsukamoto, M. Okada, and S. Komaki, "Fiber-optic radio access networks using photonic self-synchronized TDM bus link," in *Proc. The First International Symposium on Wireless Personal Multimedia Communications (WPMC'98)*, Yokosuka, Japan, pp.145-150, Nov. 1998.

[38] W. Domon, M. Shibutani, and K. Emura, "SCM optical multiple-access networks with cascaded optical modulators," *IEEE Photon. Technol. Lett.*, vol.5, no.9, pp. 1107-1109, Sept. 1993.

[39] T. Fujii, K. Tsukamoto, and N. Morinaga, "Optical multiaccess SCM/coherent detection system using cascade connected optical phase modulators," (in Japanese), *Technical Report of IEICE*, OCS93-26, pp.41-48, June 1993.

[40] P. Suwonpanich, K. Tsukamoto, and S. Komaki, "Proposal of radio-over-fiber systems using cascaded radio-to-optic direct conversion scheme," *IEICE Trans. Commun.*, vol. E83-B, no. 8, pp. 1766-1774, Aug. 2000.

[41] P. Suwonpanich, Y. Shoji, K. Tsukamoto, and S. Komaki, "Proposal of cascaded radio-optic direct conversion radio highway," in *Proc. 1997 Asia Pacific Microwave Conference (APMC'97)*, Hong Kong, vol. 1, pp. 385-388, Dec. 1997.

[42] P. Suwonpanich, Y. Shoji, K. Tsukamoto, and S. Komaki, "Study on cascaded radio-optic direct conversion radio highway using optical amplifier," in *Proc. 1998 Asia Pacific Microwave Conference (APMC'98)*, Yokohama, Japan, vol. 1, pp. 317-320, Dec. 1998.

[43] P. Suwonpanich, K. Tsukamoto, and S. Komaki, "Optimization of optical modulation indices in a cascaded radio-to-optic direct conversion radio highway," in *Proc. 1999*

Microwave Photonics (MWP'99), Melbourne, Australia, pp. 197-200, Nov. 1999.

[44] P. Suwonpanich, K. Tsukamoto, and S. Komaki, "Proposal of radio highway using cascaded radio-to-optic direct conversion scheme," (in Japanese), in *Proceeding of IEICE. Autumn Conference*, B-501, p. 502, Sept. 1996.

[45] K. Buchanan, R. Fudge, D. Mcfarlane, T. Phillips, A. Sasaki, and H. Xia, "IMT2000: Service provider's perspective," *IEEE Personal Communications*, vol. 4, no. 4, pp. 8-13 Aug. 1998.

[46] S. Wako, "ITS: R&D and perception as the open information and telecommunications infrastructure," *IEICE Trans. A.*, vol. J81-A, no. 4, pp. 467-474, April 1998.

[47] N. Moshe, B. Josef, J. L. Anthony, M. L. Israel, and K. Yishai, "Progress in externally modulated AM CATV transmission systems," *IEEE J. of Lightwave Technol.*, vol. 11, no. 1, pp. 82-105, Jan. 1993.

[48] S. Miyamoto, Y. Park, S. Komaki, "Effect of optical fiber link noise on performance of fiber-radio microcellular system," *Technology Reports of the Osaka University*, vol. 45, no. 2228, pp. 187-190, Oct. 1995.

[49] S. Benedetto and G. Olmo, "Performance evaluation of coherent optical CDMA," *Electron. Lett.*, vol. 27, no. 22, pp. 2000-2002, Oct. 1991.

[50] P. R. Prucnal, M. A. Santoro, and T. R. Fan, "Spread spectrum fiber-optic local area network using optical processing," *IEEE J. of Lightwave Technol.*, vol. LT-4, no. 5, pp. 547-554, May 1986.

[51] K. Kitayama, "Fading-free transport of 60 GHz-optical DSB signal in non dispersion shifted fiber using chirped fiber grating," *International Topical Meeting on Microwave Photonics (MWP'98)*, WB4 (Princeton, 1998).

[52] K. Kitayama and H. Sotobayashi, "Fading-free fiber-optic transport of 60 GHz-optical DSB signal by using in-line phase conjugator," *1999 Optical Fiber Conference (OFC'99)*, WD4 (San Diego, 1999).

[53] K. W. Platt, Laser Communication Systems. New York: Wiley, 1962, Ch. 4.

[54] A. Yariv, Quantum Electronics. New York: Wiley, 1988, Ch. 14.

[55] Fong T. K., Sabido IX M. J. D., Kalman F. R., Tabara M. and Kazovsky G. R, "Linewidth-insensitive coherent AM optical links: Design, performance and potential applications,"

IEEE J. Lightwave Technol., vol. LT-12, no. 13, pp. 526-534, Mar. 1994.

[56] M. Robert, D. Richard, "A novel technique for double sideband suppressed carrier modulation of optical fields," *IEEE Photonics Technol.*, vol. 7, no. 4, pp. 434-436, Apr. 1995.

[57] R. Padovani, *IEEE personal Commun.* 3Q'94 (1994) 28.

[58] T. Shiozawa, M. Shibutani, and J. Namiki, "Upstream-FDMA/downstream-TDM optical fiber multiaccess network," in *Proc. ICC'92*, pp. 105-109, 1992.

[59] C. Desem, "Measurement of optical interference due to multiple optical carriers in subcarrier multiplexing," *IEEE Photon. Technol. Lett.*, vol. 3, pp. 387-389, 1991.

[60] N. K. Shankaranarayanan and K. Y. Lau, "Transmission impairment due to optical beat interference in subcarrier multiple access networks," in *Proc. OFC'92*, p. 290, 1992.

[61] K. Okamoto, K. Moriwaki, and S. Suzuki, "Fabrication of 64x64 arrayed-waveguide grating multiplexer on silicon," *Electron. Lett.*, vol. 31, no. 3, pp. 184-186, Feb. 1995.

[62] K. Okamoto, K. Syuto, H. Takahashi, and Y. Ohmori, "Fabrication of 128-channel arrayed-waveguide grating multiplexer with 25 GHz channel spacing," *Electron. Lett.*, vol. 32, no. 16, pp. 1474-1476, Aug. 1996.

[63] J. Farre, E. Bodtker, G. jacobsen, and K.E. Stubkjar, "Dynamic range of an optical amplifier cascade in an ASK system with significant phase noise," *IEEE Photonics Technology Letters*, vol. 4, no. 12, pp. 1354-1357, Dec. 1992.

[64] Isam M.I. Habbab and Leonard J. Cimini, Jr., "Optimized performance of erbium-doped fiber amplifiers in subcarrier multiplexed lightwave," *IEEE Journal of Lightwave Technology*, vol. 9, no. 10, pp. 1321-1329, Oct. 1991.

List of Publications by the author

Publications in Journals

[A1] Pat Suwonpanich, Yukinori Suda, Katsutoshi Tsukamoto, and Shozo Komaki, "Theoretical CDNR analysis on radio-to-optic direct conversion SCM coherent radio-over-fibre system," *Optical and Quantum Electronics*, vol. 30, no. 11-12, pp. 1103-1117, Dec. 1998.

[A2] Pat Suwonpanich, Katsutoshi Tsukamoto, and Shozo Komaki, "Proposal of radio-over-fiber systems using cascaded radio-to-optic direct conversion scheme," *IEICE Trans. Commun.*, vol. E83-B, no. 8, pp. 1766-1774, Aug. 2000.

Conference Contributions

[B1] Pat Suwonpanich, Yozo Shoji, Katsutoshi Tsukamoto, and Shozo Komaki, "Proposal of cascaded radio-optic direct conversion radio highway," in *Proc. 1997 Asia Pacific Microwave Conference (APMC'97)*, Hong Kong, vol. 1, pp. 385-388, Dec. 1997.

[B2] Pat Suwonpanich, Yozo Shoji, Katsutoshi Tsukamoto, and Shozo Komaki, "Study on cascaded radio-optic direct conversion radio highway using optical amplifier," in *Proc. 1998 Asia Pacific Microwave Conference (APMC'98)*, Yokohama, Japan, vol. 1, pp. 317-320, Dec. 1998.

[B3] Pat Suwonpanich, Katsutoshi Tsukamoto, and Shozo Komaki, "Optimization of optical modulation indices in a cascaded radio-to-optic direct conversion radio highway," in *Proc. 1999 Microwave Photonics (MWP'99)*, Melbourne, Australia, pp. 197-200, Nov. 1999.

Conference Contributions (in Japanese)

[C1] Pat Suwonpanich, Katsutoshi Tsukamoto, and Shozo Komaki, "Proposal of radio highway using cascaded radio-to-optic direct conversion scheme," in *Proceeding of IEICE. Autumn Conference*, B-501, p. 502, Sept. 1996.

[C2] Pat Suwonpanich, Katsutoshi Tsukamoto, and Shozo Komaki, "Theoretical analysis of spurious-free dynamic range on radio-on-fiber systems using radio-to-optic direct conversion scheme," *Technical Report of IEICE*, MWP2000-1, pp. 1-8, Oct. 2000.